Swansea University
Prifysgol Abertawe

Hyperspectral Imaging of Electrochemically Controlled Photoluminescence of Few Layer MoS_2 in Widefield

Anupama B. Patabandi Mudiyanselage

Swansea University

Submitted to Swansea University in fulfillment of the requirements for the Degree of *MSc by Research*

September 2024

ABSTRACT

Molybdenum disulfide (MoS_2) is one of the most important two-dimensional materials, exhibiting unique electrical and optical properties as it transitions from the bulk to the nanoscale. Typically, mechanical exfoliation and chemical vapor deposition (CVD) growth methods are used to prepare MoS_2 nanosheets for optoelectronic studies and applications. However, mechanical exfoliation suffers from low yield and CVD based MoS_2 growth involves high temperatures and complex costly set-ups. Hence, electro exfoliation has emerged as a promising scalable and cost-effective technique to produce few layer MoS_2. In recent years, these MoS_2 materials have gained significant importance in catalysis, as the efficient electron transfer facilitated by excitons and trions has proven particularly beneficial for reactions such as the hydrogen evolution reaction (HER). Also, according to the past research these few layers of MoS_2 has considerable heterogeneity in their optical and electrical properties due to the presence of defects and discontinuities at the edges. Therefore, investigation of these spatial inhomogeneity is important to use these materials in the real-world applications.

The present study was divided into two steps. Firstly, a simple electrochemical exfoliation method was employed to synthesise few-layer MoS_2, avoiding the drawbacks associated with existing synthesis processes. The produced MoS_2 was then characterised using Raman spectroscopy and photoluminescence spectroscopy to ensure the material's quality and structural integrity. Secondly, these produced few layer MoS_2 was used to observe the change of the photoluminescence intensity across a single MoS_2 flake and the asymmetric characteristics of trion photoluminescence with applied voltage using in-situ electrochemical setup. Hyperspectral imaging was employed, capturing spectral features from each pixel across a broad field of view rather than individual points.

The result from the study indicates that the electro exfoliation method can produce MoS_2 flakes with two or three layers on average, and the in-situ electrochemical characterisation showed significant spatial variations and a strong dependence on the voltage, highlighting the influence of electrical layer formation on the photoluminescence from excitons and trions. Therefore, the correlation between the PL intensity variations and applied voltages provides insights into the dynamics of excitons and trions under electrochemical conditions, paving the way for future studies to explore the full potential of 2D transition metal dichalcogenide materials in catalytic applications.

DECLARATION OF AUTHORSHIP

This work has not previously been accepted in substance for any degree and is not being concurrently submitted in candidature for any degree.

Signed.....[redacted].....

Date.....07/01/2025.....

This thesis is the result of my own investigations, except where otherwise stated. Other sources are acknowledged by footnotes giving explicit references. A bibliography is appended.

Signed.....[redacted].....

Date.....07/01/2025.....

I hereby give consent for my thesis, if accepted, to be available for electronic sharing

Signed.....[redacted].....

Date.....07/01/2025.....

The University's ethical procedures have been followed and, where appropriate, that ethical approval has been granted.

Signed.....[redacted].....

Date.....07/01/2025.....

TABLE OF CONTENTS

ACKNOWLEDGEMENTS

I gratefully acknowledge Dr. Deb Roy for fruitful discussions, guidance, support and encouragement throughout my research. My sincere thanks also extended to all the members of the Dr. Roy's Research Group for their continuing support. This work would not have been possible without their cooperation and encouragement.

Especially:

- Dr. Himanshu Tyagi for his support in discussions on my research, assistance with data analysis, and training on instruments, as well as for his words of encouragement.
- Scott Richardson for help with the electrochemical cell setup and other helpful discussions

Finally, I would like to thank my parents, husband, sisters and friends for their unconditional love, support and encouragement.

LIST OF FIGURES

ABBREVIATIONS

CDW	Charge density waves
CVD	Chemical vapor deposition
DI	Deionized water
DC	Direct Current
FL-MoS_2	Few-layer MoS_2
HOMO	Highest occupied molecular orbital
HER	Hydrogen evolution reaction
HSI	Hyperspectral imaging
ITO	Indium tin oxide
LUMO	Lowest unoccupied molecular orbital
OER	Oxygen evolution reaction
PL	Photoluminescence
PVD	Physical vapor deposition
RGB	Red, green and blue
TFT	Thin-film transistors
3D	Three-dimensional
TMD	Transition-metal dichalcogenide
2D	Two-dimensional
XAS	X-ray absorption spectroscopy

CHAPTER 1 - INTRODUCTION

Molybdenum disulfide (MoS_2) has emerged as a material of great interest in recent years due to its promising role in real-world applications.[1] Its ability to support efficient electron transfer via excitons and trions makes it particularly useful for catalytic processes. However, previous studies reveal significant heterogeneity in the optical and electrical properties of MoS_2, which stems from structural defects and edge discontinuities in its few-layer configurations.[1] Investigating these spatial variations is essential for a deeper understanding of material fbehavior. This research explores how photoluminescence intensity varies across a single MoS_2 flake and examines the asymmetrical trion photoluminescence response under applied voltage using an in-situ electrochemical approach. By employing hyperspectral imaging, spectral data were collected across an extensive field of view, offering a more detailed perspective than traditional methods.

1.1 Two-dimensional (2D) materials: An overview

The landmark discovery of graphene in 2004, a single-atom-thick sheet of carbon atoms in a hexagonal lattice structure, sparked the widespread attention and intensive research into a diverse array of two-dimensional (2D) materials.[1–4] This, in turn, has driven breakthroughs across a multitude of applications, from electronics and photonics to energy storage systems.[3,4] In addition to graphene, other 2D materials such as transition metal dichalcogenides (TMDs), hexagonal boron nitride (h-BN), and phosphorene possess unique properties that have been the focus of extensive research.[2,5] Graphene serves as the fundamental building block for the development of various 2D materials, TMDs, hexagonal boron nitride (h-BN), and black phosphorus or phosphorene. 2D materials can be broadly categorised into elements, metallic compounds, non-metallic compounds, organics, and salts. Figure 1.1 illustrates the basic structure and classification of these different 2D materials.[6] Hexagonal boron nitride(h-BN) is a graphene analogue, exhibiting a crystallographic structure with boron and nitrogen atoms substituting the carbon atoms.[7] TMDs, on the other hand, have a formula of MX_2, where M represents a transition metal and X denotes a chalcogen. These TMDs possess a crystal structure characterised by a tri-layer covalent bonding arrangement, typically in the form of X-M-X.[6]

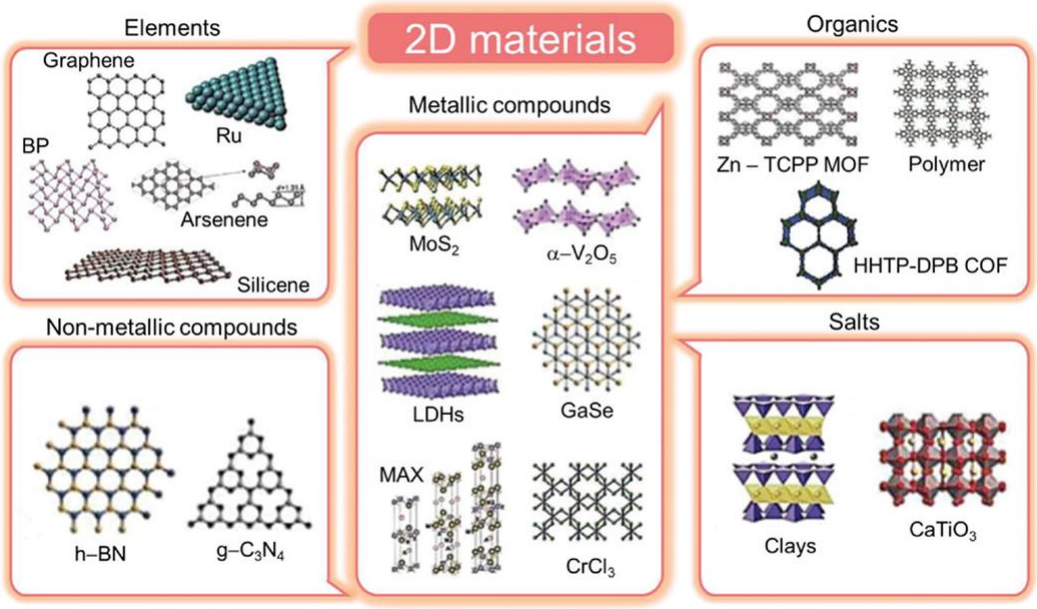

Figure 1.1: The basic structure and classification of different 2D materials.[6]

Moreover, advancements in nanotechnology have significantly altered global perspectives across diverse domains. Nanomaterials have been classified along a dimensional spectrum, from zero-dimensional (0D) quantum dots to one-dimensional (1D) nanoribbons, nanotubes, and nanowires, and finally to two-dimensional (2D) single-atom-thick materials like graphene, as well as three-dimensional (3D) structures such as nanoballs and nano cones.[8,9] The size of a material at the nanoscale has a profound impact on its properties and behavior, with electrical, chemical, mechanical, and optical characteristics significantly enhanced as the dimensions are reduced. For instance, 2D materials exhibit greater strength and a higher surface area-to-volume ratio compared to their 3D counterparts, leading to increased reactivity and a large charge storage.[10,11] These distinctive physical and chemical attributes of 2D materials have driven their extensive research and development, making them superior to the bulk materials commonly used in various applications.

Beyond their large specific surface area, 2D materials exhibit other distinctive properties, including mechanical stability, transparency, tuneable bandgap flexibility, and high packing density, which render them suitable for flexible thin-film supercapacitors.[10,11] The high surface area of 2D materials provides an enhanced surface-to-volume ratio, enabling greater energy storage per unit mass and facilitating faster ion transport between the electrode and electrolyte, thereby improving charging and discharging rates.[3,10,12] The robust mechanical strength of 2D materials, which exceeds that of other dimensional materials, enables them to withstand

environmental harsh environments, mechanical stresses, volume fluctuations, and the stresses encountered during charge-discharge cycles.[6] This collective resilience contributes to the outstanding cyclic stability of these materials. The electrical conductivity of 2D materials is also a crucial factor in determining the performance of electrochemical charge storage devices.[4,13,14] The low electrical resistance exhibited by 2D materials enables them to efficiently transport the charge carried through the interfaces. Finally, the tunability of their properties by manipulating the structure, thickness, composition, and dimensions further supports their application in energy storage.[15–18] However, the strong pi-pi interactions and van der Waals forces can lead to the restacking and aggregation of monolayers, which ultimately reduces the accessible surface area and impedes their contribution to electrochemical applications.[6,19,20] (Figure 1.2)

1.2 2D - Transition metal dichalcogenides

Two-dimensional TMDs are a class of materials that exhibit a layered structure, distinct from the structure of graphene.[14] These TMDs are composed of a transition metal layer sandwiched between two chalcogen layers, with strong covalent bonds within the plane and weak interlayer non-covalent bonds between the layers. The transition metals include elements like molybdenum (Mb), niobium (Nb), and tungsten (W), while the chalcogens include sulphur (S), tellurium (Te), and selenium (Se).[21] As such, some common examples of TMDs include, molybdenum disulfide (MoS_2), molybdenum diselenide ($MoSe_2$), tungsten disulfide (WS_2), and tungsten diselenide (WSe_2).[2,5,6] The strong covalent bonding within the planes and weaker interlayer bonding of TMDs enables the isolation of their 2D structures through various exfoliation techniques. These methods include lithium intercalation, mechanical exfoliation using adhesive tape, and chemical or solvent-assisted exfoliation.[22–24]

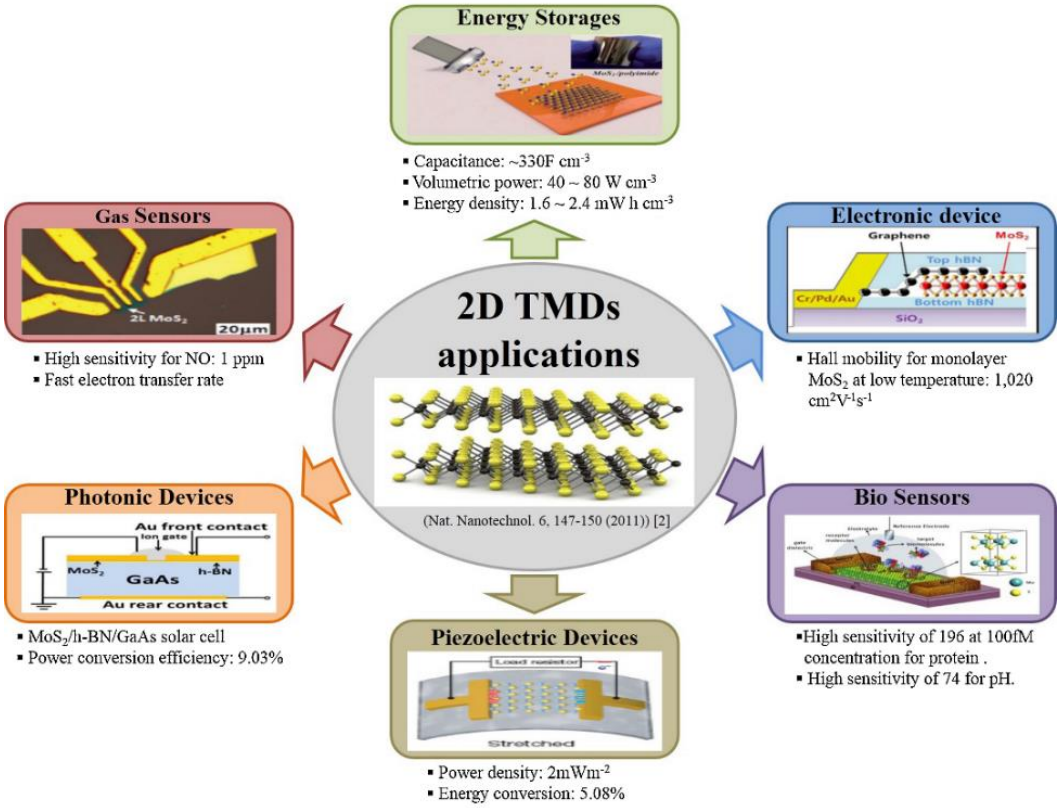

Figure 1.2: Potential applications of 2D TMDs.[21]

1.2.1 Crystal structure and physical properties of TMDs

The transition metals, including W, Mo, Re, and Ta belong to the d-block series of the periodic table and exhibit a stable oxidation state of +4. The chalcogen elements, comprising S, Se, and Te, have an oxidation state of -2. Typically, the atomic ratio in layered transition metal dichalcogenides is one transition metal atom to two chalcogen atoms, forming the MX_2 structure, although there are exceptions such as 2:3 quintuple layers and 1:1 metal chalcogenides (MXs).[25] TMDs possess a layered structure held together by weak van der Waals forces, which contributes to their lubricant properties. As illustrated in Figure 1.3a, the atoms within each layer are bonded by strong covalent interactions.[24,25]

Transition metal dichalcogenides are known to exist in various crystallographic phases, including 1H, 1T, 3R, 1T′, and 1T′′′. The numeric component in the phase nomenclature indicates the number of layers within the crystallographic unit cell, while the alphabetic element denotes the symmetry exhibited by the structure, such as T represents tetragonal (D_{3d} group), H represents hexagonal (D_{3h} group), and R represents rhombohedral (C_{3v}^5 group).[26–28] In the H-

phase structure, each metal atom exhibits six coordinated bonds, forming two tetrahedra oriented along the +z and -z directions, while maintaining a hexagonal arrangement in the top view (Figure 1.3a).[25] The chalcogen-metal-chalcogen stacking along the z-axis is considered a single layer, and the weak van der Waals interactions between these layers (chalcogen–chalcogen) enable mechanical exfoliation, facilitating the isolation of single-layer flakes from the bulk TMD material.[22-24] In contrast, the T-phase exhibits a trigonal chalcogen layer on the top and a 180° rotated structure at the bottom within a single layer, resulting in a hexagonal arrangement of chalcogen atoms in the top view. Further distortion of the metal atoms, known as the T′-phase, leads to a modification in the atomic displacement of the chalcogen atoms along the z-direction.[25] The 1T polymorph exhibits metallic properties, whereas the 2H, 3R, and 1T′ polymorphs display semiconducting characteristics.[25] In the 1H phase of MS_2 (M= W/Mo), the metal atoms adopt a trigonal prismatic coordination. Likewise, the 3R phsase demonstrates semiconducting behaviour with a trigonal prismatic arrangement of the chalcogen atoms around the metal.[25-27]

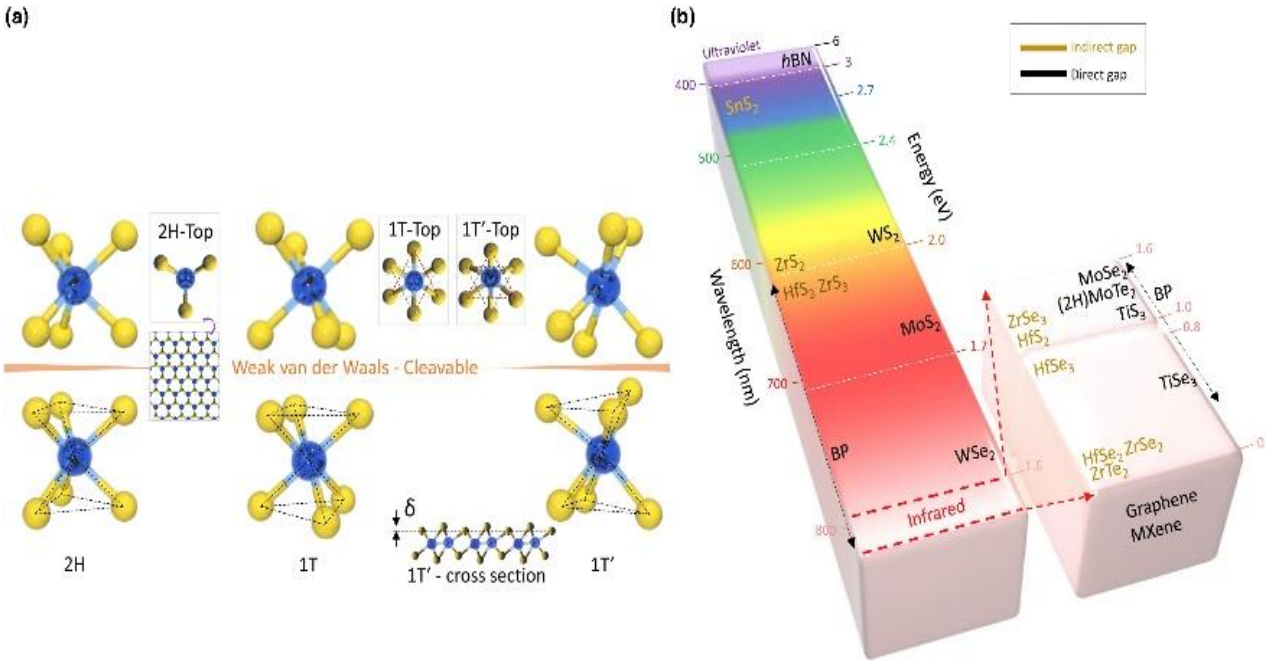

Figure 1.3: a) Hexagonal arrangement of chalcogen atoms b) Wide range band gaps of 2D TMDs in visible and infrared spectrum.[25]

As shown in Figure 1.3b, the 2D TMDs exhibit a remarkably wide range of bandgaps, covering the entire visible and infrared spectrum.[14] Interestingly, most semiconducting 2D TMDs possess a direct bandgap in their monolayer form, while transitioning to an indirect bandgap in the bulk state, with a few exceptions like GaSe and ReS_2. For instance, the monolayer forms of MoS_2 (1.8 eV), $MoSe_2$ (1.5 eV), $MoTe_2$ (1.1 eV), WS_2 (2.1 eV), and WSe_2 (1.7 eV) all display direct bandgaps, whereas their bulk counterparts exhibit indirect bandgaps with smaller energies.[25] Most MX_2 materials are free from dangling bonds thus demonstrating high charge carrier mobility. This mobility is dependent on the choice of suitable substrate and metal contacts, as well as potential suppression due to grain boundaries. For instance, MoS_2 exhibits mobilities ranging from 700 $cm^2V^{-1}s^{-1}$ on SiO_2/Si substrates with Sc contacts to 33-151 $cm^2\ V^{-1}\ s^{-1}$ on BN/Si encapsulated substrates at room temperature.[14] In addition to their excellent electrical transport properties, TMDs are also mechanically flexible and strong, comparable to graphene.[29] Suspended few-layer MoS_2 nanosheets have exhibited an exceptionally high Young's modulus of ~0.33 ± 0.07 TPa. Furthermore, studies have reported high in-plane stiffness and Young's modulus values of 180 ± 60 Nm^{-1} and 270 ± 100 GPa, respectively, for single-layer MoS_2. The Young's modulus of monolayer MoS_2 surpasses even that of stainless steel and graphene oxide, which is attributed to the absence of stacking faults, high crystallinity, and defect-free nature of these atomically thin TMDs.[30–32] In addition to their exceptional mechanical properties, TMDs also exhibit other intriguing physical phenomena, such as charge density waves (CDW), magnetism (ferromagnetic /antiferromagnetic) and superconductivity.[30,31]

1.2.2 Electrical, energy and optoelectronics applications

TMDs have garnered significant attention due to their exceptional electronic properties. These materials exhibit desirable characteristics such as flexibility, thinness, and transparency.[21,23,33] Owing to their semiconductor nature, TMDs find applications in a variety of technological domains, including memory devices, transistors, photovoltaic devices, photodetectors, lithium-ion batteries, and catalysts for hydrogen evolution reactions.[2-6] As discussed above, 2D TMDs can be classified based on their electronic characteristics, which encompass metallic, semimetallic, and semiconducting varieties. Metallic TMDs possess a high density of states at the Fermi level, resulting in high electrical conductivity. In contrast, semimetallic TMDs exhibit low electrical conductivity due to the small overlap between their valence and conduction bands, leading to a low density of states at the Fermi level.[30,34] Semiconductor TMDs have a large band

gap, but their electrical conductivity can be enhanced through doping or the application of an electric field. Furthermore, TMDs share similarities with silicon, such as a band gap in the visible-near infrared range, high carrier mobility, and high on/off ratios.[34] Additionally, TMDs can be deposited on flexible substrates while maintaining their structural integrity when subjected to stress and strain.[35–39]

One of the key features of TMDs is their tuneable bandgap, which can transition from an indirect to a direct bandgap when reduced to monolayer thickness. This property enables enhanced light absorption and emission, making TMDs suitable for applications in photodetectors, light-emitting devices, and solar cells.[37] For instance, materials like MoS_2 and WS_2 exhibit efficient PL and can be integrated into next-generation optoelectronic devices, promising improved performance over traditional materials like silicon.[33,40] Unique properties of MoS_2 include direct band gap (~1.8 eV) good mobility (~700 $cm^2\ V^{-1}\ s^{-1}$), high current on/off ratio 0f ~107 – 108, large optical absorption (~107 m^{-1} in the visible range) and a PL signal arising from the direct bandgap in monolayer. Because of these characteristics MoS_2 has been studied widely for electronic and optoelectronic applications.

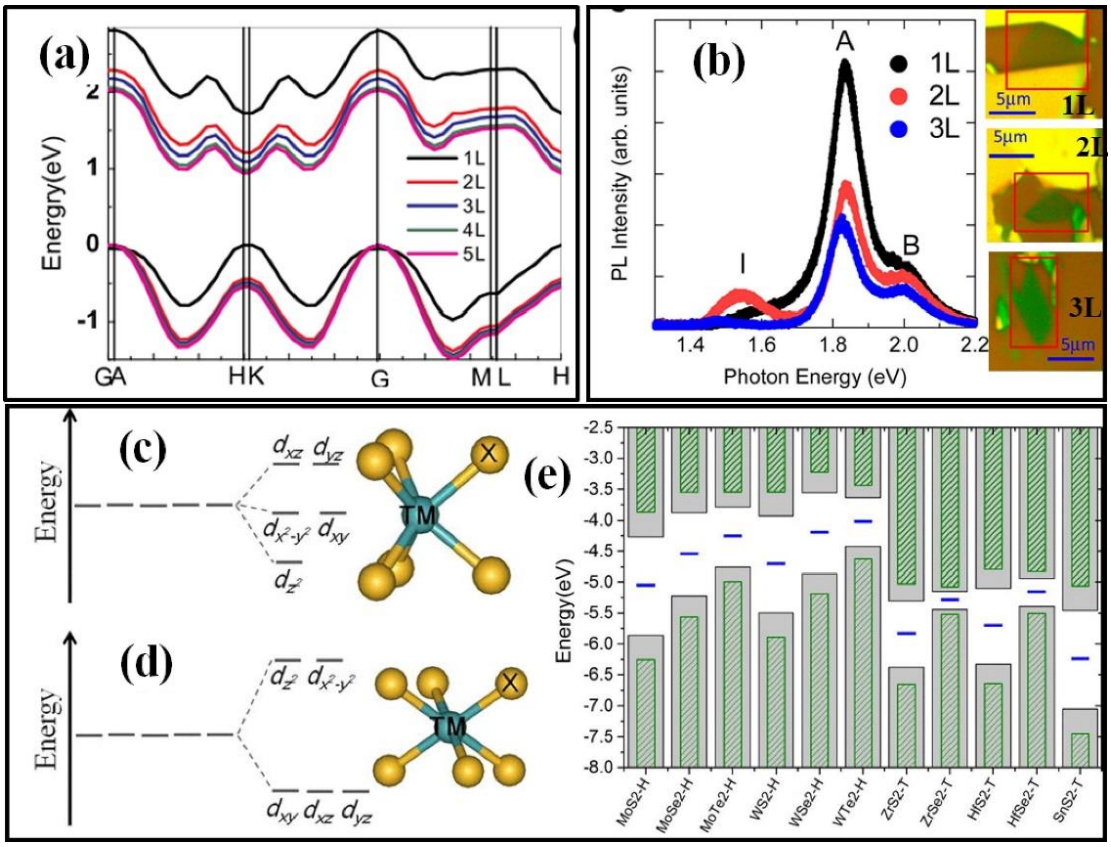

Figure 1.4: a) Electronic band structure of MoS_2 with 1–5 layer b) PL spectra of MoS_2 from one to three layer number c) Trigonal prismatic coordination d) Octahedral coordination e) Band alignment of various monolayer TMDCs.[21]

In the realm of electrical applications, TMDs demonstrate excellent charge carrier mobility and scalability, crucial for the development of high-performance transistors and integrated circuits.[21] The two-dimensional nature of TMDs allows for the fabrication of ultra-thin devices that can be layered to create complex circuits while maintaining low power consumption. These characteristics are particularly advantageous for flexible and wearable electronics, where lightweight and conformable materials are required.[13,18]

High-performance two-dimensional thin-film transistors (2D TFTs) fabricated using synthesised MoS_2 have now been reported. These MoS_2 TFTs, operating at room temperature, exhibit the characteristic high on/off current ratio and current saturation expected of high-quality TMDs.[14,41] Specifically, electron mobilities up to ~50 $cm^2\ V^{-1}\ s^{-1}$ and current densities of 250 μA/μm have been observed, which is highly promising for high-performance TFT applications. Remarkably, cut-off frequencies (the frequency beyond which the TFT's response significantly less) exceeding 5 GHz have been realised on flexible plastic substrates with

channel lengths of just 0.5 μm. While the relatively low intrinsic mobility of MoS_2 may have initially suggested this level of high-frequency performance would be challenging, it has been found that at the high electric fields required for maximum operating frequency, charge transport is instead dominated by the saturation velocity of material, which is sufficiently high to enable GHz operation in these sub-micron channel devices.[41]

TMDs also hold promise in energy applications, particularly in catalysis for hydrogen evolution and energy storage systems.[42–44] Their unique surface properties and catalytic efficiencies make TMDs excellent candidates for developing efficient electrocatalysts for water splitting, contributing to sustainable hydrogen production.[43] Moreover, TMDs have been explored in the context of lithium-ion batteries and supercapacitors, where their high surface area and electrical conductivity enhance charge storage capabilities.[41] The integration of TMDs into these energy devices can lead to improved performance metrics, such as higher energy densities and faster charge-discharge rates. As research progresses, the combined potential of TMDs in electrical, energy, and optoelectronic applications underscores their role as key materials in advancing technology towards a more efficient and sustainable future.[40-43]

Therefore, the exploration of TMDs in various domains reflects their versatility and capability to revolutionise existing technologies. With ongoing research focused on optimising their properties and exploring novel combinations with other materials, TMDs are poised to play a critical role in shaping the future of electronics, optoelectronics, and energy systems. As these materials continue to be integrated into practical applications, they offer exciting possibilities for innovation in areas ranging from communication technologies to renewable energy solutions. The potential benefits of TMDs underscore the importance of continued investment in research and development to unlock their full capabilities.

1.3 2D-MoS_2 nanomaterial

Molybdenum disulfide (MoS_2) is a prominent two-dimensional (2D) nanomaterial with significant potential across various fields, driven by its unique structural, electronic, and mechanical properties.

1.3.1 Structure of MoS_2

Molybdenum disulfide is a 2D TMD material analogous to graphene. Each individual monolayer of 2D MoS_2 measures approximately 0.65 nm in thickness and is stacked together by weak van der Waals forces to form the bulk MoS_2 material.[40,45–48] In contrast to the zero-bandgap semiconductor property of graphene, the bulk, multi-layer, and few-layer forms of MoS_2 are indirect bandgap semiconductors. However, the bandgap of MoS_2 can be converted from an indirect to a direct bandgap by reducing the material to the monolayer form.[20]

Single-layer MoS_2 is composed of two hexagonal planes of sulphur atoms separated by a plane of molybdenum atoms, forming an S–Mo–S structure.[32,36,49,50] Layered bulk MoS_2 exhibits three polymorphic crystalline forms as 1T, 2H, and 3R, which differ in their coordination environment and stacking order. Visualised from a crystallographic perspective, these three phases are depicted in Figure 1.5

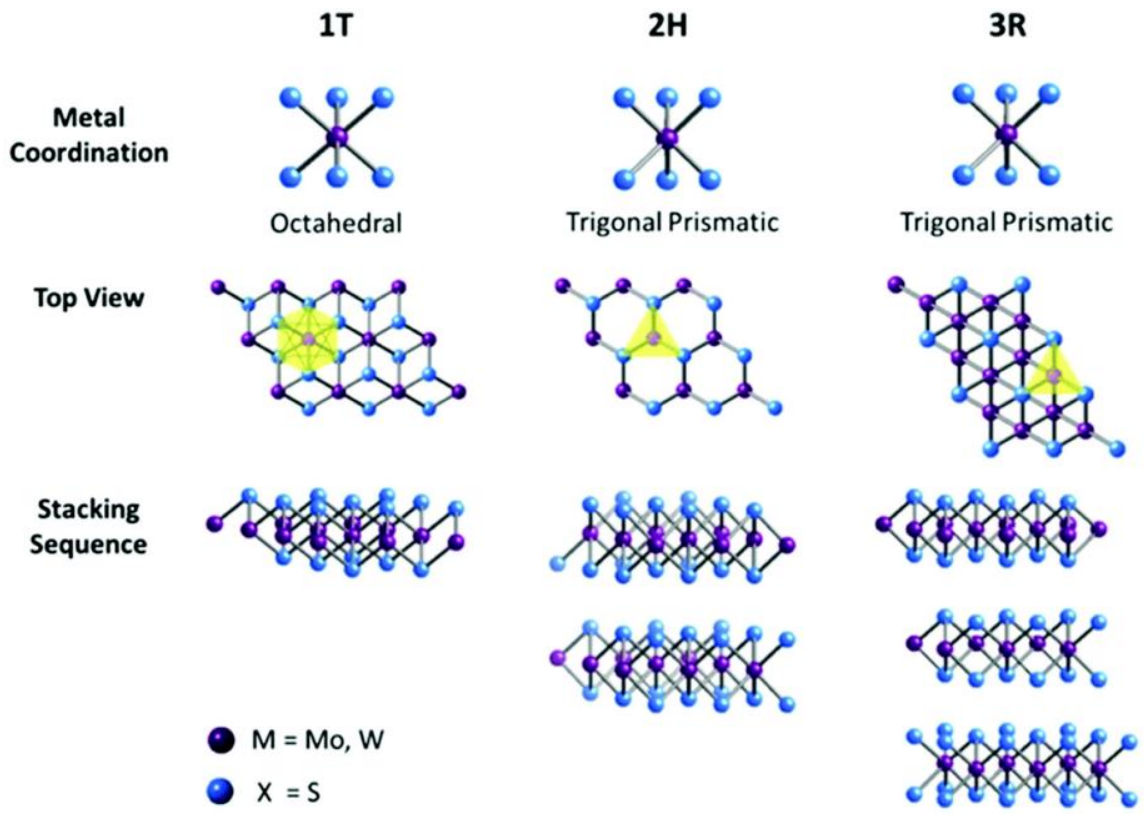

Figure 1.5: Metal coordination and stacking sequences of MoS_2.[51]

1.3.2 Preparation of MoS_2 nanomaterials: Various methods

In recent years, there has been significant progress in the synthetic techniques and processes for producing molybdenum disulfide nanomaterials. These advancements have laid a strong foundation for fundamental research and applications, considerably promoting the development of this material. The synthesis method is key to the development and use of MoS_2, with significant scientific and economic value.[52] Analogous to graphene, the preparation method for two-dimensional layered MoS_2 begins with mechanical exfoliation, and various other synthetic techniques have been developed through continuous research and exploration. The synthesis of nanoscale materials can be broadly classified into two main approaches: the top-down and bottom-up methods, as illustrated in Figure 1.6.

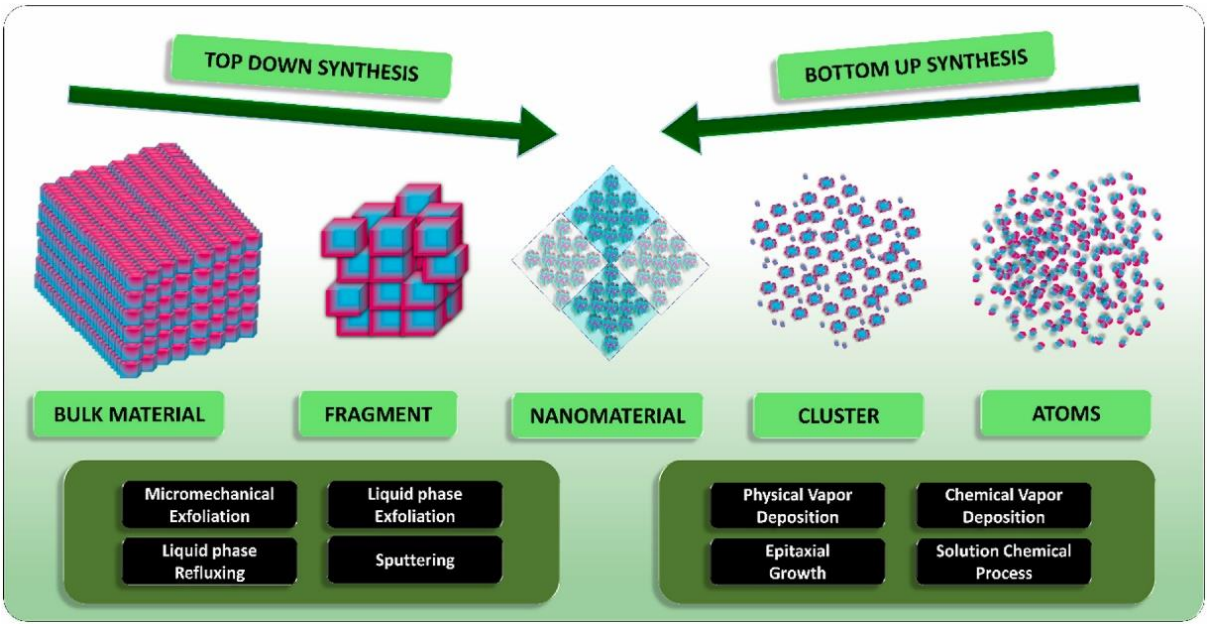

Figure 1.6: Synthesis pathway of MoS_2.[52]

Top-down approaches rely on splitting or removing bulk material or shrinking bulk manufacturing processes to produce the required structure with the appropriate characteristics.[53,54] These methods are, by nature, more straightforward. This approach encompasses techniques such as micromechanical exfoliation, liquid phase exfoliation, and sputtering. However, these top-down methods are frequently avoided due to their exceptionally low product yields. The financial constraints make large-scale synthesis of high-quality nanomaterials unfeasible through these approaches.[52,53]

One of the earliest techniques for producing sheet-like nanomaterials, such as graphene, black phosphorus, borophene, transition metal dichalcogenides, and MoS_2, is mechanical exfoliation-(Figure 1.7a). This method utilises adhesive tapes to create MoS_2 flakes on a substrate.[52] The process involves using bulk MoS_2 as the starting material, where a portion is peeled off using tape and deposited onto the substrate surface. Due to van der Waals forces on the substrate, some MoS_2 pieces remain attached after the tape is removed. Repeating this procedure yields MoS_2 flakes of various sizes on the surface. The low production efficiency and small lateral size (usually <10 μm) of the single-layer flakes obtained are major drawbacks of this method. Additionally, the discarding of Scotch tape containing the exfoliated flakes after deposition on the target substrate introduces various challenges and limitations in the isolation of individual

layers from the bulk material. Consequently, this technique suffers from poor process yield and results in significant waste of two-dimensional materials.[52,53]

Owing to its inherent scalability, liquid-phase exfoliation has recently garnered significant attention. This process involves dispersing a bulk material in a solvent, followed by the separation of the material's layers.[55] Liquid-phase exfoliation is the primary approach for generating large quantities of 2D materials, such as graphene, with a favourable balance between quality and cost, and it is now extensively utilised in both academic and industrial sectors. The force generated by ultrasound and its interaction with the solvent molecules have traditionally been considered the primary drivers of the fragmentation and exfoliation mechanisms (Figure 1.7b) Specifically, the process of ultrasonication involves transmitting high-frequency sound waves through a solution, which leads to the separation of the material's layers. As the layers expand, the bubbles and cavities created by the sound waves facilitate this separation.[52,53] However, these processes also induce stresses in the material, resulting in a reduction in the size of the particles obtained after exfoliation, as the particles are cleaved intra-layers. In addition to ultrasonication, other techniques for liquid-phase exfoliation have been developed, such as freezing water-intercalated layered structures, where the expansion of water during freezing induces cleavage between the layers, and strong acid-induced oxidation processes that also lead to cleavage.[52] After the exfoliation step, isolated particles of a specific size can be obtained through various methods, including centrifugation of the dispersion, solvent-induced selective sedimentation, or pH-assisted selective sedimentation.

The sputtering technique is a method for producing nanomaterials by bombarding solid surfaces with high-energy particles such as gas or plasma.[52-54] This process involves striking the target surface with intense gaseous ions, which physically eject small atom clusters based on the incoming gaseous-ion energy. Sputtering typically occurs within a chamber that has been evacuated and then filled with sputtering gas. In this process, a high voltage applied to the cathode target causes free electrons to collide with the gas, resulting in the formation of gas ions. These positively charged ions then accelerate rapidly in the electric field as they approach the cathode target, ejecting atoms off its surface. The sputtering conditions impact the microstructural characteristics of the deposited material, including its composition, crystallinity, and film-like morphology. Also, recent research group was demonstrated the use of magnetron sputtering to create a MoS_2 monolayer at the wafer scale in 2014, where a high-temperature

molybdenum metal target sputtered in a vaporised sulphur ambient generated the MoS_2 films.[52] A schematic representation of sputtering process is shown in Figure 1.7c.

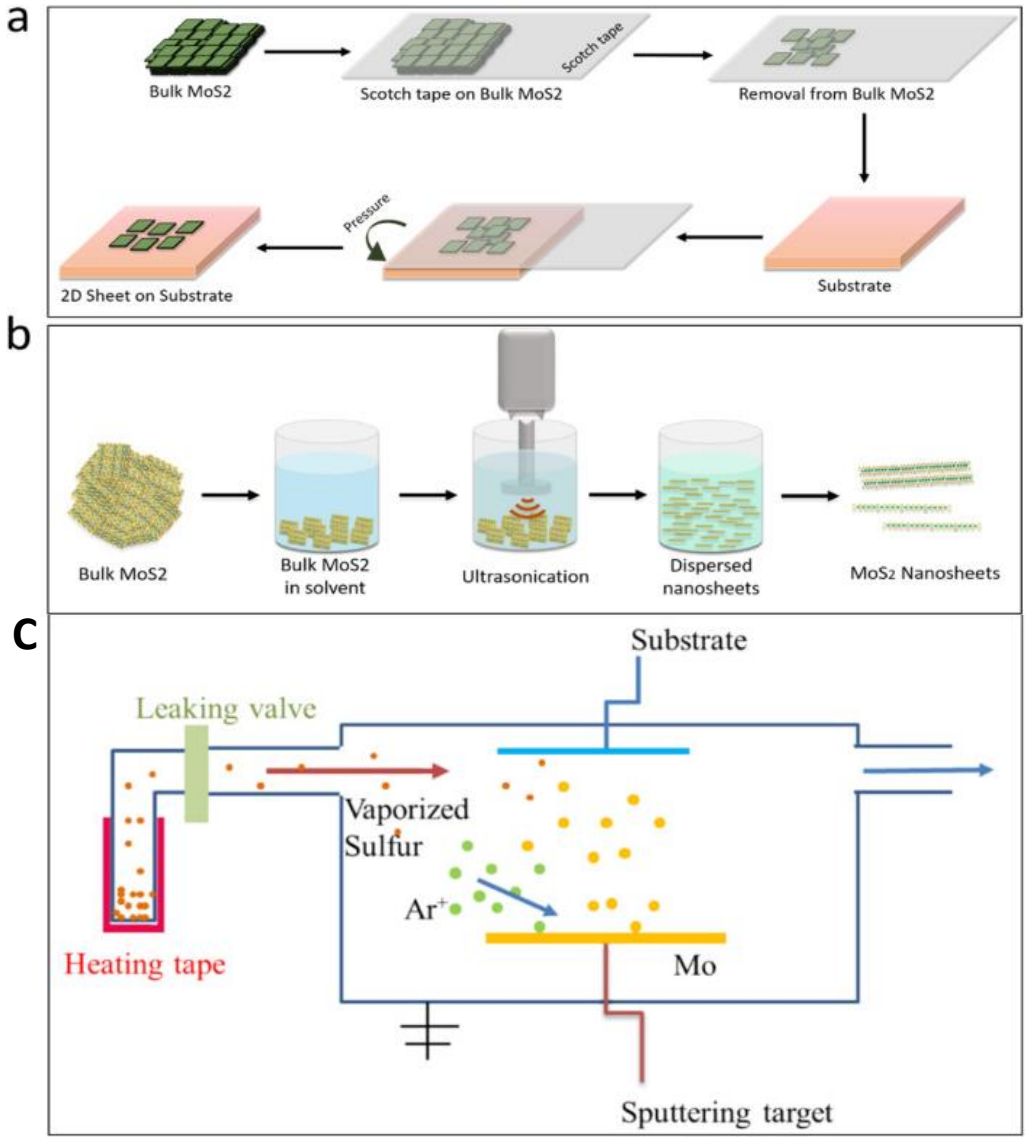

Figure 1.7: Schematic representations of different synthesis process a) Mechanical exfliation b) Liquid-phase exfoliation c) Sputtering technique.[52]

The bottom-up approach is another process for synthesising nanomaterials. In this method, atoms and molecules combine at the nanoscale to create nano-dimensional materials. This process involves scaling up materials to design the desired structure. While generally sophisticated, the hydrothermal and solvothermal synthesis procedures offer a high-yield, making them well-suited for high-performance applications. Common synthesis techniques for MoS_2-based nanomaterials include Physical Vapor Deposition (PVD), Chemical Vapor Deposition (CVD), and solution-based chemical processes.[52-54]

Generally, there are three widely employed physical vapor deposition techniques: thermal evaporation, sputtering, and arc vapor deposition. In the thermal evaporation process, the material to be coated is vaporised using a heated coil.[52] The [lower method relies on the impact of gaseous plasma on a target material to dislodge atoms for deposition on a substrate. The arc vapor deposition process utilises an electric arc to vaporise the material. The goal of PVD is to vaporise a material and then uniformly distribute the vapor over a suitable substrate.[52,53] This synthesis technique is highly sophisticated and expensive. One challenge is producing MoS_2 substrates with minimal energy consumption. Although a previous research study demonstrated the preparation of 3-6 layer MoS_2 molecular films on a SiO_2 substrate at a temperature of 350 °C, lower energy consumption is expected to enable upscaling of the synthesis process.[52]

Unlike the physical vapor deposition process, where solid material is vaporised to produce the gaseous source, the chemical vapor deposition technique utilises a gaseous precursor.[54] During the CVD process, the film is generated entirely based on the chemical reaction between the reacting gases and the substrate. This synthesis method is also a relatively high-cost technique. However, the CVD technique is an ideal choice for fabricating high-performance electronic devices. Figure 1.8a illustrates a typical CVD process, where the unreacted products are eliminated using a carrier gas.[52,54] The versatility of the CVD method allows for the preparation of various types of material structures. As shown in Figure 1.8b, the CVD process can generate vertically and planarly aligned MoS_2. The synthesis procedure can be tailored to create the desired structural differences. For the preparation of MoS_2 using CVD, molybdenum is used along with a source of sulphur, and they are reacted with each other under the required gas flow and temperature conditions.[52,53]

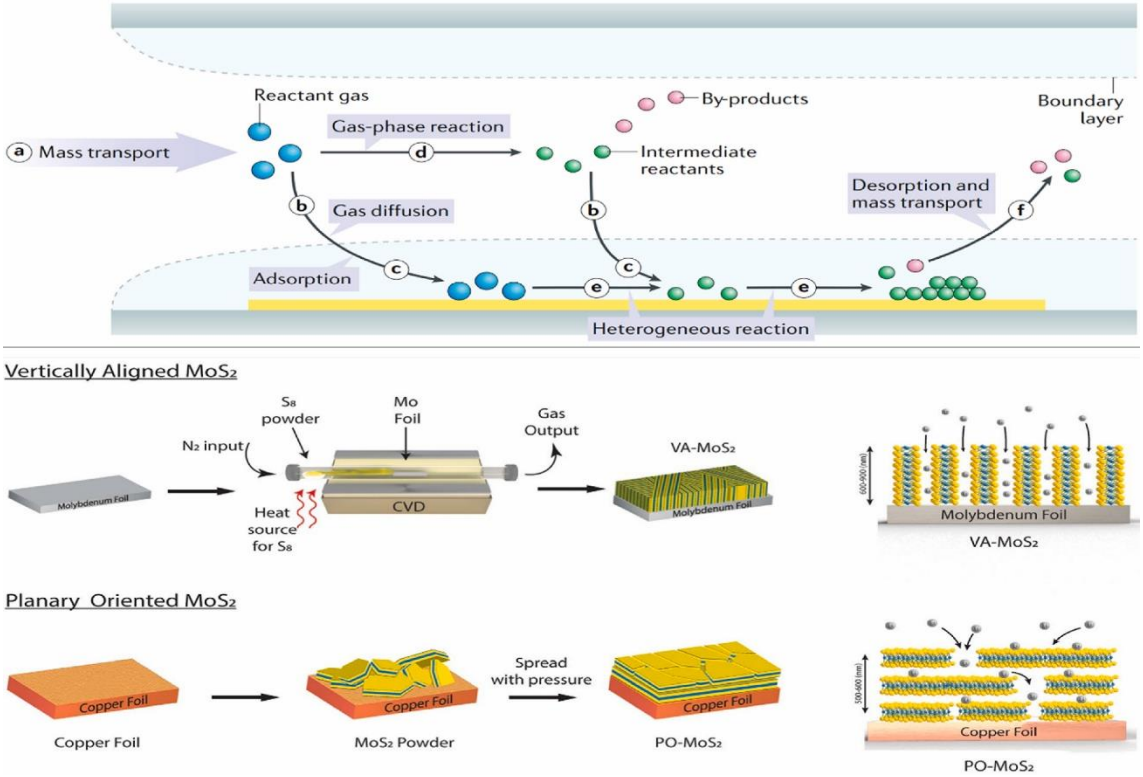

Figure 1.8: Schematics of CVD method a) Reaction pathways of typical CVD process b) Two methods of CVD process; vertical aligned and planary oriented.[52]

1.3.3 Preparation of MoS_2 using electrochemical exfoliation method

Realising the versatile potential applications of 2D materials require the development of efficient and cost-effective industrial-scale production methods to fabricate high-quality samples. As discussed above various top-down techniques, including scotch-tape isolation, chemical exfoliation, and liquid-phase exfoliation, have been explored to produce layered 2D materials[52]. However, these top-down methods have drawbacks, such as being time-consuming, utilising hazardous chemicals, and generating defects.[52,53] In contrast, bottom-up approaches, such as epitaxial growth and chemical vapor deposition, can prepare large-area ultrathin 2D materials. Yet, these bottom-up processes are complex, costly, and require high temperatures and vacuum conditions. Moreover, an additional transfer step is needed to move the 2D products from the metal surface to the target substrates, which complicates the manufacturing process and may introduce impurities or defects into the 2D materials. Compared to other fabrication methods, electrochemical approaches typically operate under mild conditions, making them

more convenient and controllable. Electrochemical exfoliation of layered bulk materials, such as through anodic oxidation–cationic intercalation or cathodic exfoliation, involves using a liquid electrolyte and applied potential to drive structural expansion. This is a promising approach to scalable exfoliating 2D materials.[15,22,23] The layered bulk materials have strong in-plane covalent bonds, but weak out-of-plane bonds held together by van der Waals interactions. These weak bonds can be easily broken by cations or anions under highly negative or positive charge, allowing the materials to be exfoliated down to atomically thin 2D forms.

According to the differences in exfoliation electrodes, the preparation of MoS_2 nanosheets through electrochemical exfoliation can be categorised into anode exfoliation, cathode exfoliation, and other electrochemical exfoliation methods.[52] Anode exfoliation involves using bulk MoS_2 as the anode and a platinum wire or foil as the cathode in dilute H_2SO_4 and Na_2SO_4 solutions. This process is similar to the anode exfoliation of graphene and formation of oxygen-containing free radicals and the generation of gases are the two key factors for achieving anodic exfoliation (Figure 1.9a).[21]

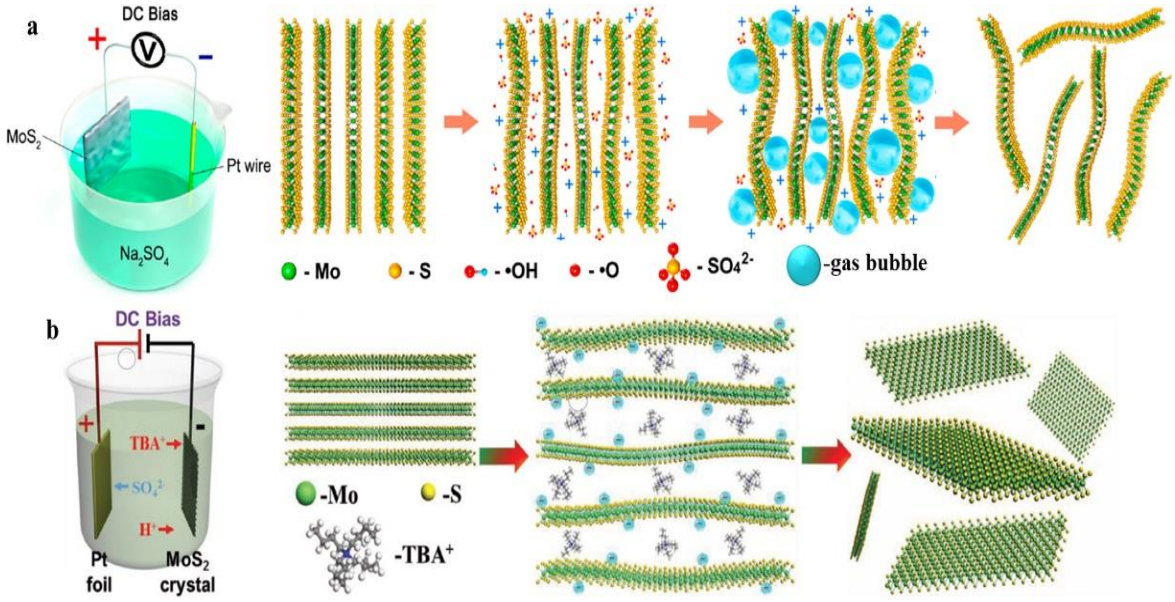

Figure 1.9: Schematic of electroexfoliation methods a) Anodic exfoliation b) Cathodic exfoliation.[52]

The cathodic exfoliation approach for producing MoS_2 nanosheets utilises bulk MoS_2 crystals as the cathode and platinum wires or foils as the anode, with the process occurring in either an organic solution of long-chain ammonium salts or an aqueous solution of inorganic salts such as K_2SO_4, NaCl and KCl. This exfoliation method is analogous to the electrochemical cathode

exfoliation of graphene in terms of the underlying process and mechanism.[52] The MoS_2 nanosheets are isolated and suspended in the electrolyte due to the force of gas evolution (Figure 1.9b) Therefore, the selection of a suitable electrolyte to facilitate both the intercalation of cathode ions and the generation of gas is crucial for achieving successful cathode exfoliation. Additionally, the use of an organic solvent for the cathode exfoliation avoids the formation of unstable 2H-MoS_2 that can occur during the anode exfoliation process.[53]

1.3.3.1 Advantages and limitations of the MoS_2 exfoliation approach.

Electrochemical exfoliation can produce high-quality, defect-free MoS_2 nanosheets with excellent purity, which is crucial for applications requiring high-performance materials. The method is scalable, making it suitable for large-scale production, and is relatively inexpensive compared to other methods like chemical vapor deposition (CVD) and mechanical exfoliation.[51,52] Additionally, electrochemical exfoliation is environmentally friendly, often using aqueous electrolytes and generating fewer harmful by-products. Its versatility allows it to exfoliate a variety of materials, not just MoS_2, making it a versatile technique for nanomaterial synthesis.[52]

However, achieving uniform thickness in the exfoliated nanosheets can be challenging, which can affect the material's properties and its suitability for certain applications. The choice of electrolyte can significantly impact the quality and yield of the nanosheets, and finding the optimal electrolyte can be a complex and time-consuming process.[14,56] While electrochemical exfoliation generally produces high-quality materials, there is still a risk of introducing defects during the exfoliation process, which can affect the electronic and mechanical properties of the material. Furthermore, the mechanisms underlying electrochemical exfoliation are not fully understood, making it difficult to optimise the process for different materials. In summary, electrochemical exfoliation offers a cost-effective, scalable, and relatively environmentally friendly method for synthesising high-quality MoS_2 nanosheets, but challenges such as controlling nanosheet thickness and optimising electrolyte selection need to be addressed to fully realise its potential.

1.4 Motivation, aims and objectives

Recent studies have demonstrated the potential of MoS_2 and other 2D transition metal dichalcogenides as promising candidates for various electrochemical applications, including hydrogen evolution reaction, oxygen reduction reaction, and supercapacitors. For instance, the concentrations of excitons and trions in 2D TMD semiconductor catalysts are modulated by electrolyte gating during electrocatalytic reactions, which also depends on the doping type. n-type semiconductors favour cathodic reactions such as the hydrogen evolution reaction, while p-type semiconductors favour anodic reactions such as the oxygen evolution reaction. Typically, 2D TMD semiconductor catalysts consist of a mix of 'active' and 'inert' sites, and the effects of electrolyte gating on these sites during electrocatalytic reactions are not fully understood. Therefore, in-situ electrochemical characterisation of these materials will provide a detailed understanding of the dynamic behaviour of excitons and trions under voltage differences. Hence, using these understanding identify the changes in exciton dynamics and find the relationship between voltages and optical behaviour to optimise the electrochemical performance is the aim of this research.

The general objectives of this research were twofold: First, to develop a simple and cost-effective method for synthesising FL-MoS_2 nanosheets through electrochemical exfoliation of bulk MoS_2 crystals. Second, to investigate the characteristic photoluminescence features of the resulting MoS_2 flakes, including the total photoluminescence, B-excitons, A-excitons, and trions, and to correlate these properties with the applied electrochemical potential. Additionally, hyperspectral imaging was employed throughout the experiments to capture real-time changes in the photoluminescence intensity of the MoS_2 samples. A key objective was to identify and investigate the trion-rich 'hotspot' regions, and to monitor how the distribution and characteristics of these trion-dominated areas varied with the applied voltage.

CHAPTER 2 - RESEARCH BACKGROUND

2.1 Electrochemical studies and findings of MoS_2

Since the discovery of MoS_2, extensive research efforts have been focused on transitional metal sulfides, particularly nanoscale MoS_2 and MoS_2-based materials, as they show promise as inorganic electrocatalysts for hydrogen evolution reaction (HER) due to their low cost, high chemical stability, and excellent electrocatalytic properties.[48,57–59] MoS_2 is a semiconductor with a bandgap of 1.2-1.8 eV and an indirect absorption edge at over 800 nm, which is favourable for solar light harvesting also there is a prominent difference in conductivity to the active sites on MoS_2 nanoplates and nanoparticles.[2,60] This leads to the identification of two potential applications of MoS_2 in photoelectrocatalytic HER (i) the use of MoS_2 as both the semiconductor and the photoelectrocatalytic HER catalyst and (ii) the use of an alternative semiconductor in combination with MoS_2 as the photoelectrocatalytic HER catalyst.[42]

Pristine MoS_2 exhibited poor catalytic performance due to the limited number of exposed active sites and its semiconducting nature.[24,26] To enhance the catalytic performance, it is crucial to focus on increasing the intrinsic catalytic activity, creating more active sites, and improving the electrical conductivity. Efforts have focused on increasing the concentration of these active edge sites to enhance the performance of the electrodes (Figure 2.1).

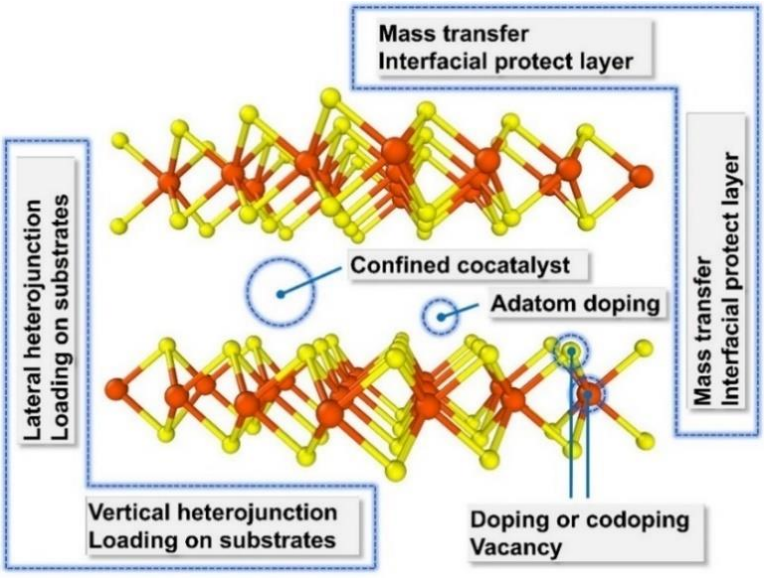

Figure 2.1: Modifications and design strategies to improve reaction performance of MoS_2 .[62]

Researchers have employed phase and structural engineering methods, such as modulating crystallisation and fabricating nanostructures, to enhance the conductivity or activity of the pristine catalysts.[62] Additionally, loading these catalysts on conductive substrates has been used to modulate the current density distribution. Edge, vacancy, and boundary regions have been identified as inherent catalytic sites.[62] Furthermore, the introduction of dopants and the formation of heterojunctions have been successful strategies to construct a larger number of active sites.[50,62–64] According to the past research the low-coordinated edge sites show moderate hydrogen adsorption behavior, which facilitates the water splitting reaction. Some studies have demonstrated that interlayer expansion can adjust the H adsorption energy and modulate the catalytic performance.[62] The pristine, well-coordinated basal plane was initially inert in the hydrogen evolution reaction; however, researchers found that introducing vacancies on the basal plane or forming grain boundaries could activate the HER catalytic ability of the otherwise inert basal plane. Comparative studies have revealed that the catalytic performance of the edge sites is superior to that of vacancies or boundaries, particularly in terms of kinetics.[62,63]

The catalytic activity of MoS_2 edge sites can be further enhanced by loading the catalyst onto a suitable support material. Studies have shown that support can significantly influence the hydrogen binding energy through long-range van der Waals interactions, leading to improved hydrogen evolution reaction performance.[62] Additionally, modulating the interlayer spacing of MoS_2 can alter the local chemical environment and electronic structure, providing another avenue to elevate the catalytic activity of the edge sites.[62-64]

Doping and heterojunction engineering have emerged as widely adopted strategies to enhance the catalytic performance of MoS_2.[62,65–67] These approaches can induce various beneficial effects, such as creating new catalytic sites by activating the inert basal plane, introducing vacancies, or incorporating exotic catalytic sites.[66] Moreover, they can improve the material's conductivity by increasing the electronic carrier density or inducing phase changes, and simultaneously enhance the reaction kinetics. Therefore, both the overpotential and Tafel slope can be improved together.[67] Compared to edge, boundary, or vacancy engineering, the doping and heterojunction methods are more versatile in adjusting the structure and catalytic performance of MoS_2. The heterojunction in particular, can modulate the intermediate adsorption to elevate the reaction kinetics or introduce various exotic catalytic sites or promoters. This approach has been successfully employed to fabricate catalysts with superior alkaline HER performance.

2.2 Electrochemical Cyclability and Reactions with NaCl as an Electrolyte

MoS_2 exhibits interesting electrochemical behavior when used in systems with NaCl as the electrolyte. Applying a voltage of 10V introduces notable effects on both the material and the electrolyte due to high electric fields, which can influence ion dynamics, electrochemical reactions, and stability. At this voltage, the interactions between Na^+, Cl^- ions, and the MoS_2 structure become more intense, enabling specific reactions but also increasing the risk of side effects such as corrosion or structural degradation.[66] At 10V, the electrochemical system experiences heightened ion mobility and reaction rates. The primary reactions involving MoS_2 include sodium ion intercalation and deintercalation, which are important for its electrochemical cyclability. Reduction reaction at cathodic sites, sodium ions are driven into the MoS_2 lattice during the reduction process, facilitated by the high voltage. Also, during oxidation Reaction at anodic sites, sodium ions are released regenerating the MoS_2 structure.[66-68] These reactions highlight material ability to handle ion intercalation and deintercalation, making it a robust candidate for cycling stability. However, at 10V, significant attention must be given to the electrolyte itself. In NaCl, chloride ions can undergo oxidation to produce chlorine gas

$$2Cl^- (aq) \longrightarrow Cl_2 (g) + 2e-$$

This reaction becomes prominent at higher potentials, such as those near or exceeding 10V. The generation of chlorine gas can lead to localized pH changes, corrosion of nearby components, and even partial damage to the MoS_2 lattice.[66] Furthermore, the Electrochemical stability of the system can depend on the pH of the electrolyte solution. At a neutral pH (around 7), the environment is generally less corrosive, and MoS_2 remains stable. However, side reactions during electrochemical cycling can alter the pH.

Water splitting reactions at higher voltages:

$$2H_2O (aq) + 4e^- \longrightarrow 2H_2 (g) + 4OH^- (aq) \quad \text{(Cathodic reaction, increases pH)}$$

$$2H_2O (aq) \longrightarrow O_2 (g) + 4H^+ (aq) + 4e^- \quad \text{(Anodic reaction, decreases pH)}$$

Fluctuations in pH, particularly toward acidic levels due to the generation of H^+ ions at the anode, can exacerbate MoS_2 oxidation and degradation. Maintaining a controlled pH, ideally

buffered near neutral, is critical to ensuring the stability of MoS_2 and reducing corrosive effects on the material and electrodes.

2.3 Importance of in-situ characterisation method on MoS_2

MoS_2 exhibits a range of catalytic sites, such as edges, vacancies, 1T basal planes, and dopants, though the specific mechanisms operating on these sites have not been well observed.[42] Moreover, the true active structure of the catalyst should be identified during actual electrocatalysis, as the catalyst structure and coordination can self-adjust during the catalytic reactions. Steady-state and post-test characterisation results are unconvincing for revealing the active catalyst structures, as MoS_2 structure is sensitive to changes in electron density, and distorted phases are thermodynamically unstable.[16,68,69] Studies have found that the structure of amorphous MoS_2 can transform during electrocatalysis, with the 1T phase converting to the 1T' distorted phase.[42] Other types of MoS_2 electrocatalysts may also undergo structural self-reconstruction, particularly in terms of vacancies, and the distorted 1T-related phases are especially vulnerable under high current densities.[68]

In-situ and operando characterisation techniques with atomic-scale spatial and temporal resolution should be employed to provide more detailed insights into the mechanistic aspects, enabling the catalytic performance on the various sites to be directly tracked, which will aid in the development of superior electrocatalysts. Furthermore, characterisation should focus on the near-surface and interfacial regions, and investigate the interplay between the bulk, near-surface, and interface. Interfacial reactant and product transport, as well as the interfacial electric double-layer structure, are not easily monitored, and their influence on catalytic performance remains poorly understood.

Current in-situ tools, such as scanning electrochemical microscopy, often lack the spatial resolution needed to observe changes at the nanoscale, where many catalytic reactions occur.[42] Enhancing the resolution and sensitivity of in-situ tools is essential for capturing transient phenomena, such as the formation of active sites or intermediate species during reactions. For instance, previous research have already demonstrated the potential of providing atomic-level insights into MoS_2 under working conditions.[69] Additionally, combining in-situ techniques with complementary operando methods, such as XAS and electrochemical impedance spectroscopy, enables a more comprehensive understanding of both the material's structure and the reaction

kinetics.[67,68,69] Advanced data analysis, including machine learning algorithms, can aid in interpreting the complex datasets generated from in-situ studies, revealing the correlations between the material's dynamic behavior and its electrochemical performance. These advancements will contribute to the development of MoS_2-based materials with superior stability, activity, and efficiency for energy applications.

Different cell setups can be used in electrochemical in situ characterizations, and most experiments include a reference electrode. The use of a reference electrode offers significant advantages, such as providing stable and consistent potential for measuring the working electrode's potential, ensuring precise control and reproducibility of results. This is essential for obtaining accurate data on reaction kinetics, electrode potentials, and current-voltage relationships. However, reference electrodes also have drawbacks, including added complexity to the setup, maintenance requirements to prevent contamination, and potential limitations in spatial resolution due to their size and placement. In cases where the study's focus is not on precise voltage measurements, a reference electrode may not be necessary. In the present research, the primary goal was to visualize variations in photoluminescence across MoS_2 under applied voltage rather than to measure exact electrochemical potentials. Excluding the reference electrode simplified the setup and allowed the study to focus on capturing hyperspectral imaging data to analyze spatial changes, prioritizing the visualization of material behavior without the need for absolute voltage measurements.

2.3.1 Raman spectroscopy

Raman spectroscopy is a powerful analytical technique used to obtain information about the chemical structure, phase, morphology, crystallinity, and interactions of materials. This instrument is frequently employed for various analytical purposes.[70] The theory behind Raman spectroscopy is based on the inelastic scattering of monochromatic light, usually from a laser source. When a sample is illuminated by a certain color or wavelength of light, a tiny fraction of the scattered light exhibits a different color than the incident light.[71,72] This shift in the scattered light is related to the vibrational energy levels of the molecules that compose the sample. Rayleigh scattering is an example of elastic scattering, where the frequency of the scattered photon is the same as the incident photon.[70] Raman scattering is known as inelastic scattering. There are two types of Raman scattering: Stokes and anti-Stokes. Stokes scattering

occurs when the incident photon interacts with the sample and loses energy, resulting in a longer wavelength than the incident light (Figure 2.2). In contrast, anti-Stokes scattering happens when the incident photon interacts with the sample and gains energy, leading to a shorter wavelength than the incident light. Stokes scattering is typically more intense than anti-Stokes scattering.[70-72]

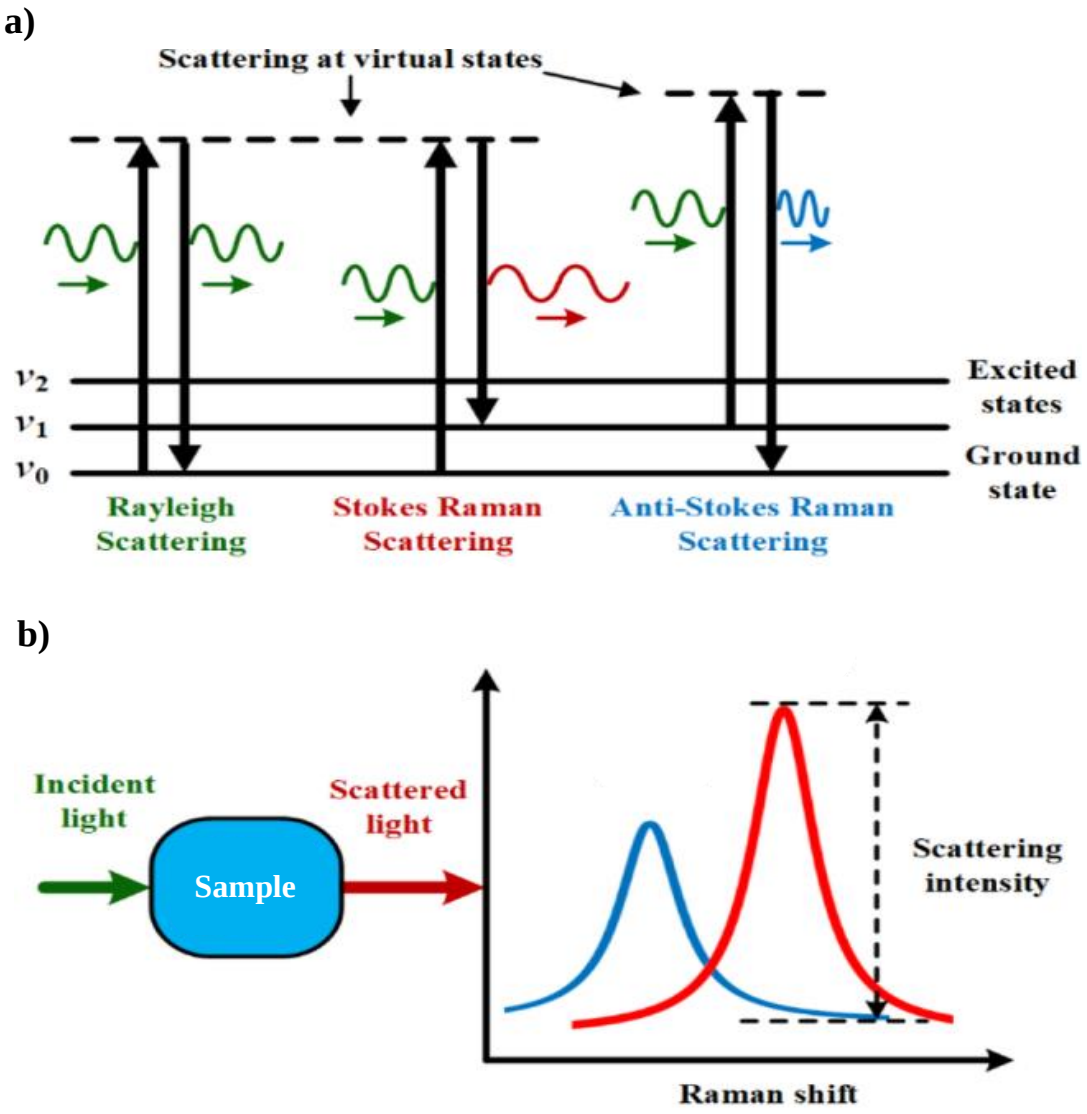

Figure 2.2: a) Energy diagram showing Raman scattering b) Different peak positions of the Raman scattering.[70]

The change in wavelength is unique to the sample, providing information about its chemical structure.[70] The Raman spectrum shows peaks with varying intensities, corresponding to molecular vibrations and individual bonds.[70] By analysing these spectral data, detailed information about the sample can be obtained. Raman shifts and relative intensities of the

Raman bands can be used to identify the material. Changes in individual bands, such as shifts, narrowing, broadening, or intensity changes, provide insights into the molecular environment and intermolecular interactions.[72] Although the Raman effect is very weak compared to other infrared spectroscopy techniques, making it invisible to the naked eye, it offers numerous advantages, including being non-destructive, highly specific, requiring no sample preparation, and allowing for rapid analysis, making it a popular choice among analytical scientists. Raman spectroscopy systems typically include a monochromatic light source, lenses to focus the laser on the sample and collect the scattered light, filters to eliminate non-Raman scattering, a diffraction grating or prism to split the light, a highly sensitive detector, and software to control the system.[71,72] The selection of the wavelength depends on the application. For example, when analysing organic materials, longer wavelengths are more suitable, as lower wavelengths can induce photoluminescence, which can prevent or obscure the Raman scattering signal.[70]

2.3.2 Photoluminescence (PL) spectroscopy

Recent research has mainly focused on layer-dependent variations in the band structure of TMDs, particularly focusing on the optical and optoelectronic characteristics. Photons with energy exceeding the bandgap can be readily absorbed due to the direct bandgap.[73,74] Consequently, there is a distinct change in the photoluminescence, absorption, and photoconductivity spectra of ultrathin MoS_2 films, especially in the monolayer form.[52] This property enables the potential utilisation of MoS_2 in optoelectronic applications. The radiative process of photoluminescence has been extensively studied, both in its static and dynamic aspects. This has been contributing significantly to the understanding of the photochemical behaviour of compounds and materials at the molecular level.[75]

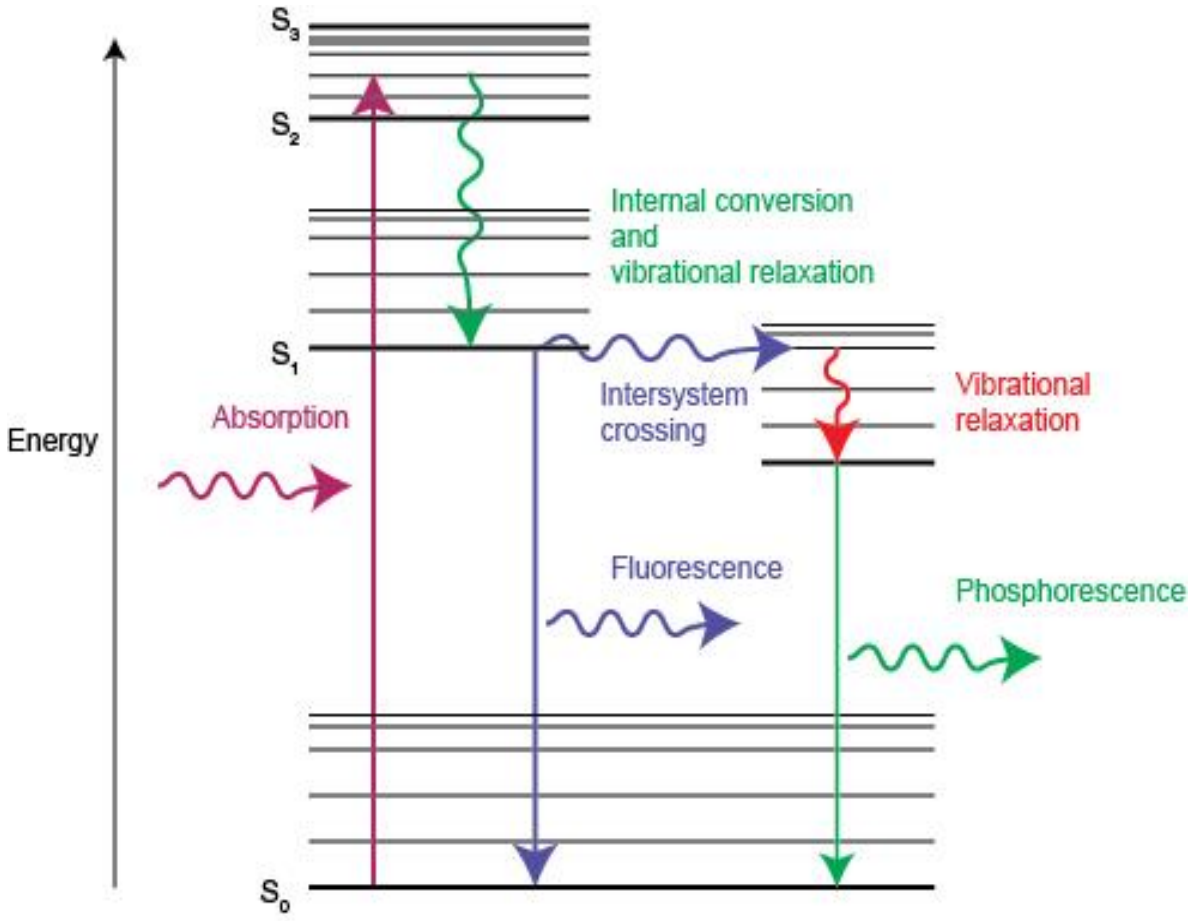

Figure 2.3: Energy diagram showing absorption of light, and the process involved in the emission of light as fluorescence and phosphorescence.[74]

The main theoretical principles that PL spectroscopy uses are fluorescence and phosphorescence.[73-75] (Figure 2.3). There are numerous pathways by which the system can revert to a lower energy state.[74] The excess energy can be depleted through vibration, rotation, and translation of the surrounding molecules or ions.[73] This energy loss is most efficient for gases and liquids, and less so for solids, where vibrations predominate due to hindered rotations and translations.[75] This thermal degradation transforms the excitation energy into thermal motion of the environment, resulting in the generation of heat. Another possibility is that the excess energy becomes involved in a chemical reaction, leading to photochemical processes. Moreover, radiative relaxation is another possible pathway, which transpires when the molecule or ion pair sheds its excitation energy through the emission of a photon.[73] Two distinct radiative

decay processes can occur, and they are known as fluorescence and phosphorescence. The radiation released during a transition between states sharing the same spin multiplicity is termed fluorescence, while the radiation released during a transition between states of differing spin multiplicity is termed phosphorescence.[75] The energy of the emitted photons directly reflects the energy difference between the participating orbitals or energy bands. This allows for determining the direct band gap in semiconductors or the HOMO-LUMO gap in molecules.[75]

PL spectroscopy can be conducted in-situ and during real-time electrochemical processes, which may offer valuable insights into defect formation occurring on surface oxidation and in oxide films subjected to electrochemical treatment.[74,75] PL spectroscopy can be used to investigate the electronic structure of traditional semiconductors like silicon when they are in contact with liquids. Overall, photoluminescence is a beneficial technique for characterizing semiconductors in solution.[75]

In the PL spectrum of MoS_2, the A and B excitons are key features that play an important role in understanding the optical properties of these materials.[73] The A exciton corresponds to the optical transition between the valence band and the conduction band at the K point of the Brillouin zone, and it is the most prominent feature in the PL spectrum. The A exciton is typically observed around 1.8 eV (650–670 nm) for monolayer MoS_2 and is strongly influenced by the spin-orbit coupling, which results in a split of the exciton levels.[73,74] The B exciton, on the other hand, arises due to a similar transition, but it corresponds to a different spin configuration and appears at a slightly higher energy, around 2.0 eV (600 - 610 nm) for monolayer MoS_2. The splitting of the A and B excitons is a direct consequence of the intrinsic spin-valley coupling and symmetry breaking in MoS_2.[73]

In addition to the A and B excitons, trions are another feature that appears in the PL spectra of MoS_2, particularly under conditions of high carrier concentration. Trions are quasi-particles formed by the binding of an exciton with an additional charge carrier, either an electron (negative trion) or a hole (positive trion).[73-75] These trion states lead to new peaks in the PL spectrum, typically observed at lower energies than the A exciton. The negative trion typically appears below the A exciton peak, while the positive trion appears below the B exciton peak. Trions are sensitive to the carrier concentration, which makes them useful for studying charge carrier dynamics and electrostatic effects in MoS_2-based devices.[75]

2.3.3 Hyperspectral imaging of FL-MoS_2

Hyperspectral imaging is a technique that provides detailed spatial and spectral information by capturing a complete spectrum for each pixel in an image, unlike traditional imaging methods that only record intensity at discrete wavelengths.[76] Hyperspectral imaging produces a three-dimensional data cube, with two dimensions representing spatial information and the third dimension containing the spectral data for each pixel (Figure 3.4). This cube enables precise spectral identification of materials, making it widely used in remote sensing, medical diagnostics, and material characterisation.

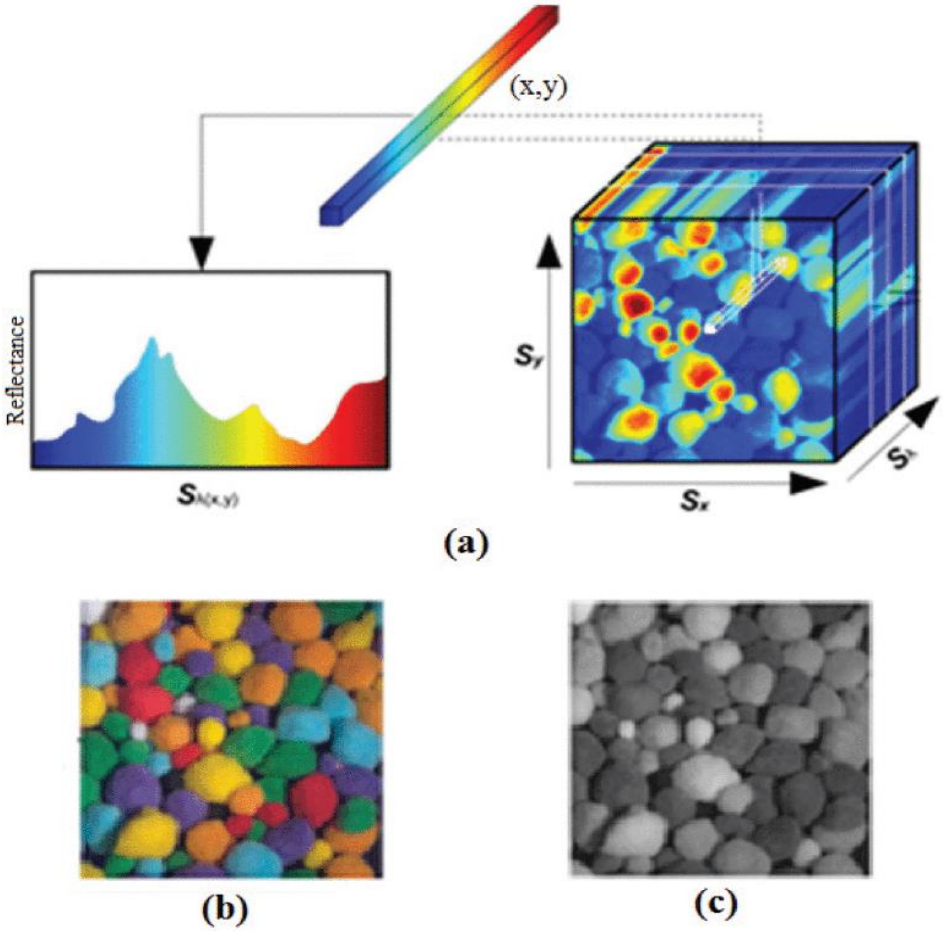

Figure 2.2.4: a) A hyperspectral image represented as a 3D cube. A point spectrum on the spectral cube is illustrated at the spatial location (x,y) b) An RGB image c) A grayscale image rendered from the hyperspectral cube.[76]

CHAPTER 3 - METHODOLOGY

3.1 Materials

Molybdenum crystal and Platinum (Pt) wire were purchased from Sigma Aldrich. Sodium sulfate (Na_2SO_4) ≥ 99.99% trace metals basis and sodium chloride (NaCl) ≥ 90.00% were purchased from Sigma Aldrich. All chemicals were used without further treatment. Distilled water (H_2O) was used as the solvent to dissolve the Na_2SO_4 and NaCl.

3.2 Synthesis of FL-MoS_2 : Electrochemical exfoliation

FL-MoS_2 sample was prepared using an anodic electrochemical exfoliation method. A natural MoS_2 crystal clamped to a Pt wire ring was used as the working electrode and immersed in a 0.5 M Na_2SO_4 solution, which served as the electrolyte throughout the exfoliation (Figure 2.1). Another Pt wire was used as the counter electrode, placed 2 cm away from and parallel to the MoS_2 crystal. The electrochemical exfoliation was carried out by applying a positive DC bias to the working electrode. Initially, a low positive bias of +2 V was applied for 10 minutes to wet the MoS_2 crystal. This was then increased to +10 V for 1-2 hours to exfoliate the MoS_2. After 2 hours, the successful exfoliation and the presence of MoS_2 flakes was evident by the appearance of pale-yellow colour of the solution. The production of air bubbles on the surface of the MoS_2 crystal is also a clear indication that the exfoliation process is taking place successfully. Furthermore, throughout the exfoliation process the Pt ring was placed approximately 3 mm above the liquid level to avoid direct contact with the electrolyte solution, which helped maintain optimal reaction conditions and prevented potential interference with the exfoliation mechanism. As the final step the exfoliated MoS_2 flakes were collected by filtration and drop-cast onto a conductive indium tin oxide (ITO) coated glass substrate for further characterisation.

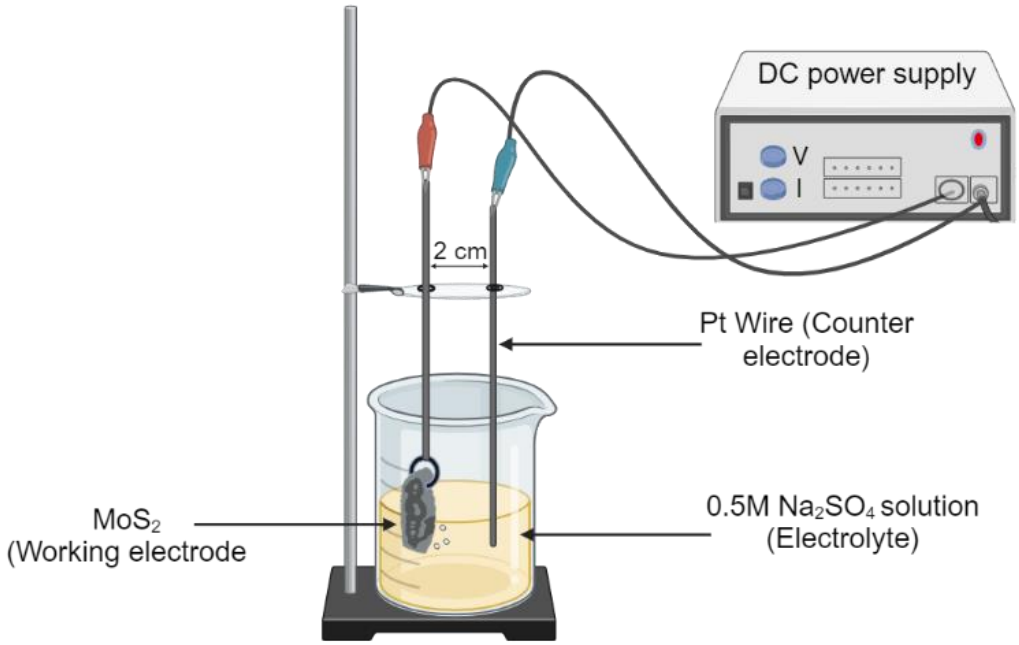

Figure 3.1: Schematic representation of elecrochemical exfoliation setup.

3.3 In-situ electrochemical study of exfoliated MoS_2 nanomaterials

The electrochemical cell was assembled using two disc-shaped outer shells made of non-reactive materials (Figure 3.2). Each disc contains a 1 cm diameter opening in the center. The top of the lower shell holds the prepared sample with the conductive substrate and acts as the anode. To provide electrical connection throughout the experiment, a clean copper plate was placed on top of the conductive substrate. A thin Pt wire was placed inside the lower shell, immersed in the electrolyte solution, and served as the cathode electrode (Figure 3.3).

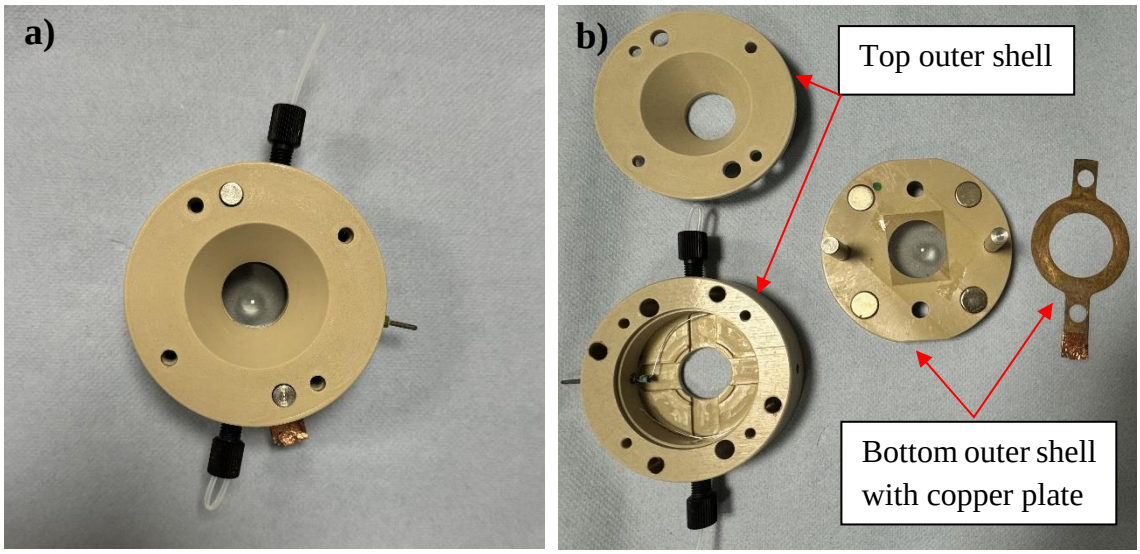

Figure 3.2: Pictures of the electochemical cell a) Top view of the cell b) Top and lower outer shells with the copper plate.

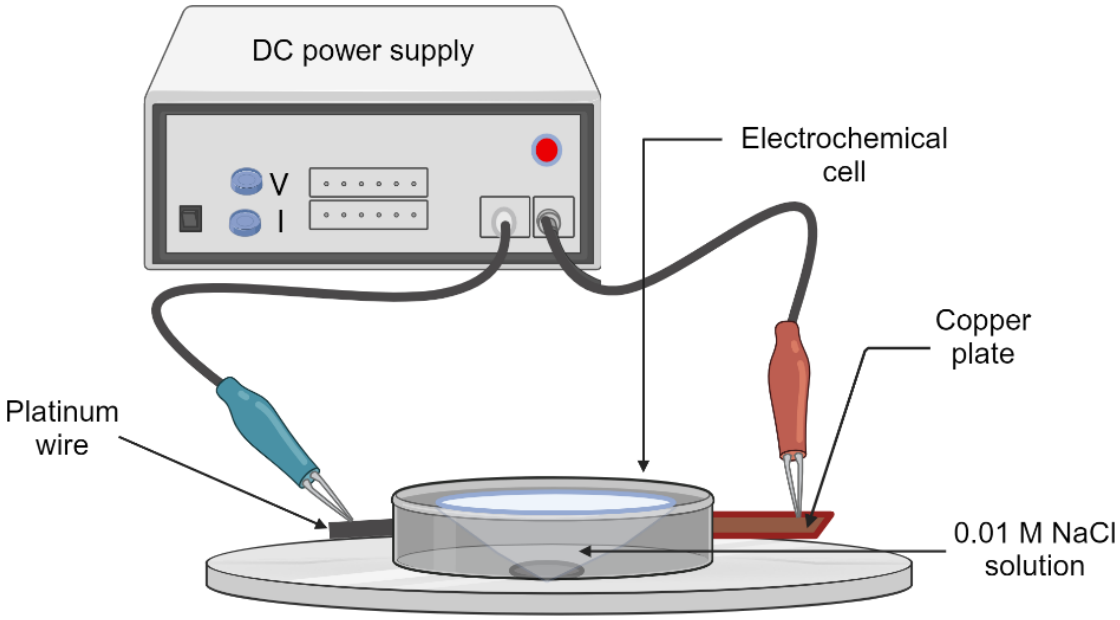

Figure 3.3: Schematic representation of elecrochemical cell setup.

Hyperspectral imaging was carried out using a customised inverted microscope (Figure 3.4). The sample was illuminated using a 532 nm laser focused at the back focal plane of the objective lens. The wide-field PL signals from the sample was collected using a high-magnification 100X oil immersion objective (1.3 NA), and Rayleigh scattering was removed by using a 540 nm long pass filter. The obtained PL signal was passed through a birefringent crystal interferometer (model: Gemini from Nireos), and the interferograms generated by the interferometer at the camera (Hamamatsu ORCA-Fusion Digital CMOS camera C14440-20UP) were Fourier transformed using a MATLAB code to generate a hyperspectral cube. The hyperspectral PL cubes obtained for various applied voltages were then used to extract different wide-field images.

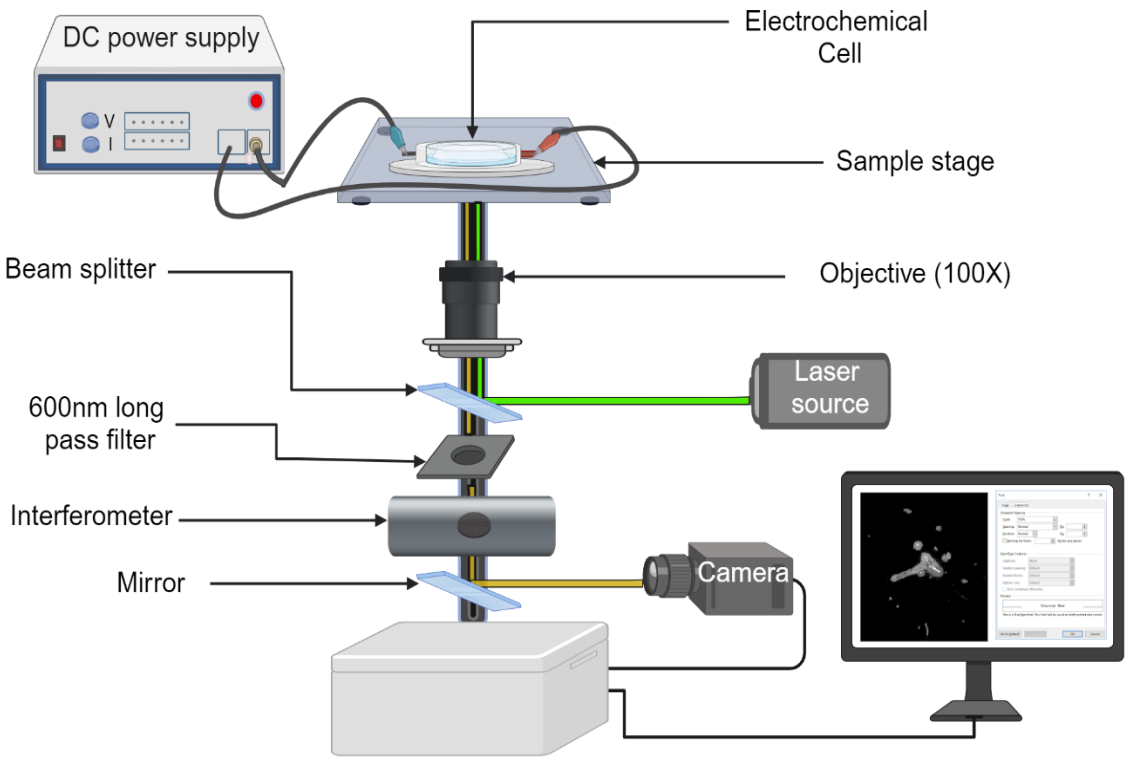

Figure 3.4: Schematic representation of microscope set up and the electrochemical cell.

3.3.1 Photoluminescence measurements using potentiostat

The prepared ITO substrate with MoS_2 sample was placed in the same two-electrode cell setup describe in above HIS imaging method. Voltages ranging from 0.8V to -0.8 V were applied across the configuration using a DC power supply. To better understand the electrolyte solution behaviour, two sets of data were collected, one using DI water and the other using a 0.01 M aqueous NaCl solution. Conventional potentiostat methods were employed to record the PL intensity changes in the two electrolyte systems during the experiment and PL differences across the flake extract from the using MATLAB code. To directly observe the trion intensity variation with voltage, a bandpass filter (680 ± 5 nm) was used.

3.3.2 Raman Spectroscopy measurements

Raman spectroscopy was employed to characterize the vibrational properties of the MoS_2 samples. The measurements were conducted using a Horiba spectrometer (monochromator with 1200 lines/mm grating) model equipped with a 540 nm laser as the excitation source. The laser power was set to 2.5 mW to minimize sample degradation, and the beam was focused onto the sample surface using a 100X magnification objective lens.

Samples were prepared by depositing thin flakes of MoS_2 onto a ITO glass. The Raman spectra were collected in the range of 350 to 4000 cm^{-1}, with a spectral resolution of 25cm^{-1}. Measurements were performed at room temperature under ambient conditions. Multiple points across each sample were analyzed to ensure reproducibility and to identify any spatial inhomogeneity in the Raman signal. The characteristic peaks of MoS_2 were identified and their positions, intensities were analyzed to infer information about layer number, strain, and other properties. All data was processed using Origin and MATLAB software. Also, baseline correction was applied to remove fluorescence interference. The results were compared to theoretical and literature values to validate the findings

CHAPTER 4 - RESULTS AND DISCUSSION

4.1 Synthesis of FL-MoS_2 nanocomposite by electrochemical exfoliation

The progression of this study was constrained by several practical challenges, primarily time limitations and sample availability. Due to the limited duration of the project, it was not possible to conduct all the necessary characterization methods such as Atomic force microscopy (AFM), Scanning electron microscopy (SEM) and X-ray diffraction analysis (XRD) to comprehensively analyze the material. Furthermore, the amount of MoS_2 sample produced during the experiments was insufficient for more extensive analyses. While the characterization techniques employed provided valuable insights, additional methods would have offered a deeper understanding of the material properties. However, the limited sample quantity and necessity to concentrate on essential experimental goals resulted in the use of only a few techniques, leaving some analyses for future investigations.

The mechanism of electrochemical exfoliation of bulk MoS_2 crystals is described in Figure 4.1. First, by applying a positive bias to the working electrode, the oxidation of water produces •OH and •O radicals that assemble around the bulk MoS_2 crystal. These •OH and •O radicals, and/or SO_4^{2-}anions, insert themselves between the MoS_2 layers, weakening the van der Waals interactions. Second, the oxidation of the radicals and/or anions leads to the release of O_2 and/or SO_2, causing the MoS_2 interlayers to greatly expand.[22] Finally, the erupting gas detaches MoS_2 flakes from the bulk crystal, suspending them in the solution. Electrochemically exfoliated MoS_2 dispersion is pale yellow colour. Although, the yellow color of the solution also can be the Pt salt in solution. making it challenging to confirm the presence of MoS_2 using conventional visual inspection. However, the Tyndall effect, a scattering phenomenon caused by particles in suspension, was employed as an effective method to detect MoS_2 in the solution. (Figure 4.2) When a laser beam was passed through the solution, the scattering of light indicated the presence of particles, confirming MoS_2 inclusion in the mixture. Despite the utility of the Tyndall effect for quick detection, traditional characterization techniques such as scanning electron microscopy (SEM), or X-ray diffraction (XRD) should be used to further verify the

material identity and ensure that the observed scattering is indeed due to MoS_2. These techniques provide more accurate and reliable data regarding the material composition, structure, and quality. Thus, while the Tyndall effect offers an initial indication of MoS_2 particles, comprehensive verification through established methods is essential to validate the findings to investigate the quality and the properties of the final product.

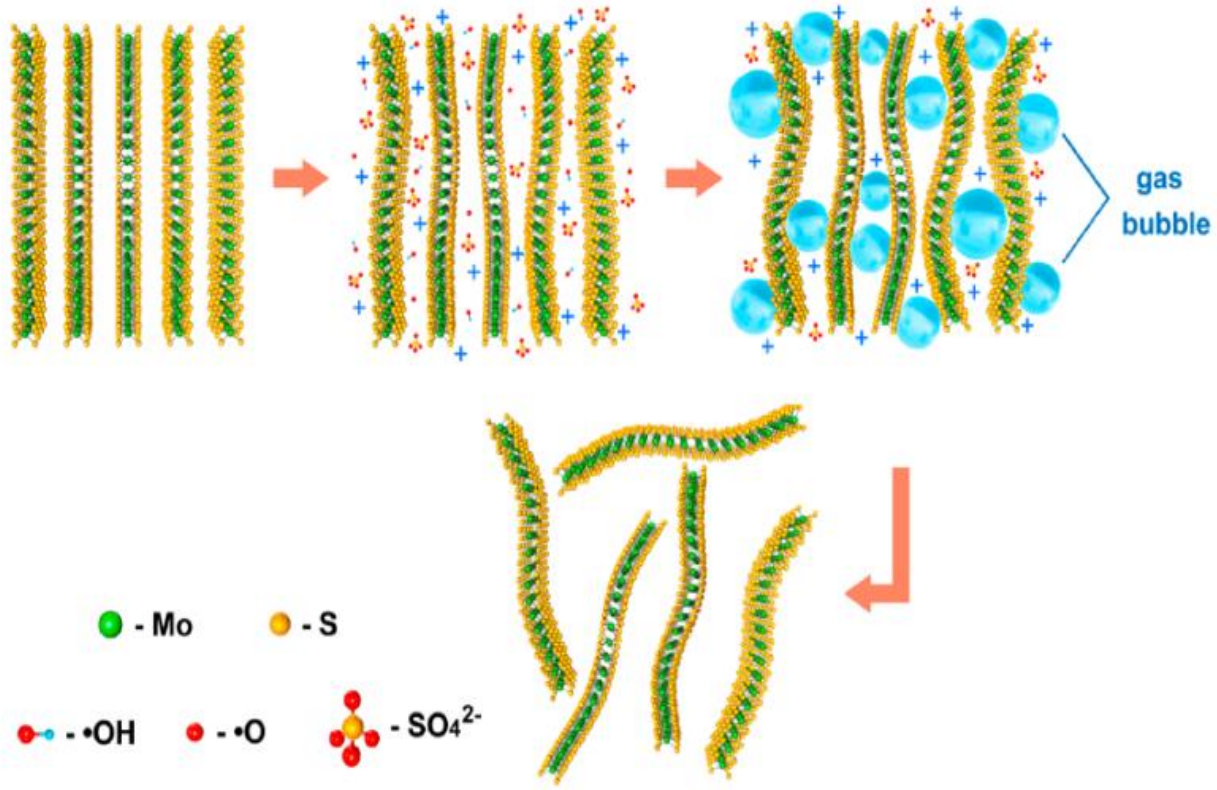

Figure 4.1: Schematic representation of anodic electrochemical exfoliation during the reaction.[52]

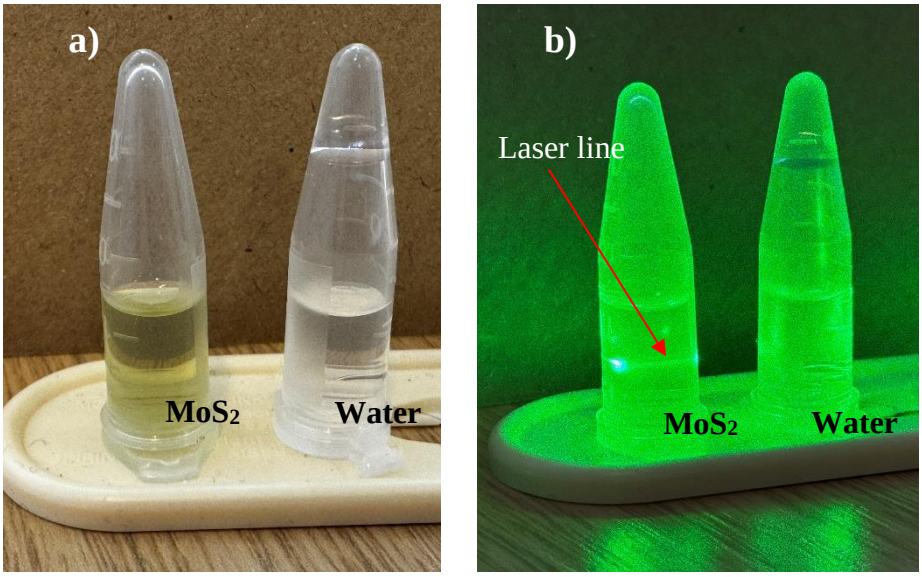

Figure 4.2: a) Before the laser beam passed through b) Laser beam passing through the solution

4.1.1 Characterisation of FL-MoS_2 using Raman spectroscopy

In the Raman spectroscopy of MoS_2, the two prominent vibrational modes that are of primary interest are the E^1_{2g} mode and the A_{1g} mode.[77] E^1_{2g} mode corresponds to the in-plane vibration of the molybdenum (Mo) and sulphur (S) atoms, where the atoms vibrate parallel to the plane of the material and the A_1g mode correspond to the out-of-plane vibration of sulphur atoms, where the vibrations are perpendicular to the plane (Figure 4.3).[27]

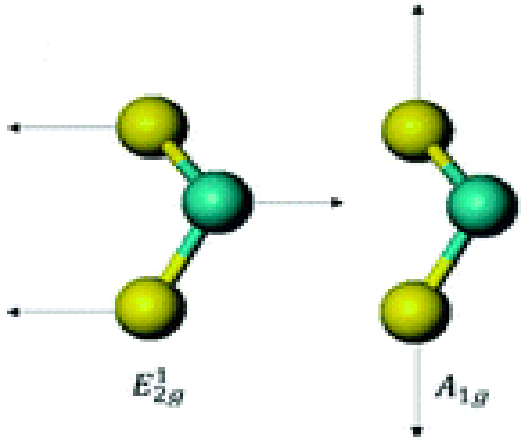

Figure 4.3: Two vibrational modes of MoS_2. Yellow color represents the S atoms and green color represent the Mo atom. [27]

According to the previous research Raman spectra of the FL-MoS_2 flakes exhibit these characteristic peaks, but their positions shift based on the number of layers in the sample.[22,75] The typical shifts observed in the Raman spectra for MoS_2 are the E^1_{2g} mode shifts to lower frequencies as the number of layers increases and the A_1g mode shifts to higher frequencies as the number of layers increases. Therefore, these shifts allow for the determination of the number of MoS_2 layers and the difference in the peak positions between the E^1_{2g} and A_{1g} modes ($\Delta\omega = \omega_{a1}g - \omega_{e2}g^1$) provides a reliable way to measure the thickness of the flake.[22] If the difference is less than 19 cm^{-1}, the sample is likely to consist of monolayers of MoS_2. Differences in the range of 20–22 cm^{-1} typically indicate a few-layered MoS_2 structure. When the difference exceeds 25 cm^{-1}, it is indicative of bulk MoS_2.[22]

In the present study, these two prominent Raman vibrational modes of E^1_{2g} and the A_{1g} can observe around 380 cm^{-1} and 400 cm^{-1} respectively (Figure 4.4). As the number of layers increases, the A_{1g} mode gradually shifts to higher wavenumbers due to stronger interlayer interactions, while the E^1_{2g} mode shifts downward due to weakened restoring forces for in-plane vibrations in thicker flakes. These shifts are subtle but consistent, confirming that the material consists of a FL-MoS_2, and those are most likely 3-5 layers based on the peak separation of 20cm^{-1} observed. Also, The FWHM (full width at half maximum) values of the E^1_{2g} and A_{1g} Raman peaks were observed 4.2 cm^{-1} and 5.1 cm^{-1} respectively. These values are indicative of few-layer MoS_2 and are consistent with the literature values reported for exfoliated samples, which typically fall within the range of 3–6 cm^{-1} for E^1_{2g} and 5–7 cm^{-1} for A_{1g}.

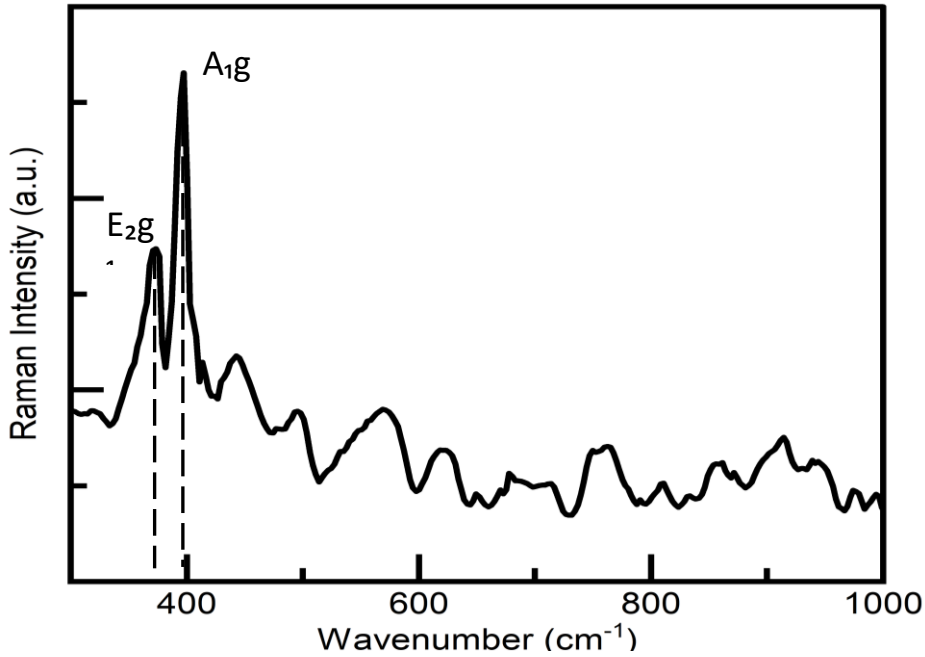

Figure 4.4: Raman spectrum of MoS_2

Furthermore, the Raman spectroscopy technique is highly responsive to mechanical strain and structural defects in materials like MoS_2. These factors can lead to visible changes in the position, intensity, and shape of the Raman peaks, which then provide insights into the mechanical and structural characteristics of the sample. As example during the exfoliation process, substrate interaction can significantly alter its Raman spectra. Strain affects the atomic bonding in the MoS_2 lattice, leading to shifts in the vibrational modes.[22,75] Although, the sharp and well-defined E_{2g}^1 and A_{1g} Raman peaks indicate (Figure 4.4) that the MoS_2 flakes in the sample experienced minimal mechanical strain. If significant strain were present, Raman spectrum expect to observe more pronounced shifting of the E_{2g}^1 mode and consistent spectral shifts across the entire Raman spectrum in the strained regions. Additionally, localised strain can lead to peak splitting or asymmetry, particularly in the E_{2g}^1 mode, as adjacent areas undergo different levels of mechanical stress. However, the absence of such peak splitting or asymmetry in the Raman data supports the conclusion that the MoS_2 flakes in this study were subject to uniform and minimal mechanical strain.[11] Defects in the MoS_2 crystal structure can arise from various factors, including imperfections of crystal lattice, missing atoms, grain boundaries, and doping.[65] These defects influence the material's vibrational modes and overall crystalline symmetry, which can be detected using Raman spectroscopy. Typically, defects cause broadening of the Raman peaks due to the disruption of phonon coherence over long distances. In contrast, pristine MoS_2 exhibits sharp and well-defined Raman peaks, indicating its long-range crystalline order. The present study suggests that the electrochemically exfoliated MoS_2 flakes have a relatively low defect density, as evidenced by the sharpness of the Raman peaks, preserving the long-range order of the crystal structure.

Additionally, the use of the interferometer-based hyperspectral imaging technique in this study resulted in a relatively lower spectral resolution compared to traditional Raman spectroscopy methods. As shown in Figure 4.5, a broad Raman band centered at 558 cm^{-1} can be observed. This corresponds to the overlap of the E^1_{2g} and A_{1g} Raman peaks of MoS_2, forming a single broad Raman feature. This overlap occurs due to the limited spectral resolution of the current setup, which is unable to distinguish peaks separated by approximately 20 cm^{-1} , as its spectral resolution is 25 cm^{-1} . This limitation made it challenging to clearly differentiate between the E^1_{2g} and A_{1g} Raman peaks when analyzing the hyperspectral data. Consequently, detailed analysis and interpretation of the Raman spectra obtained from the hyperspectral imaging were somewhat restricted due to this constraint in spectral resolution, and the data were not used in further analyses.

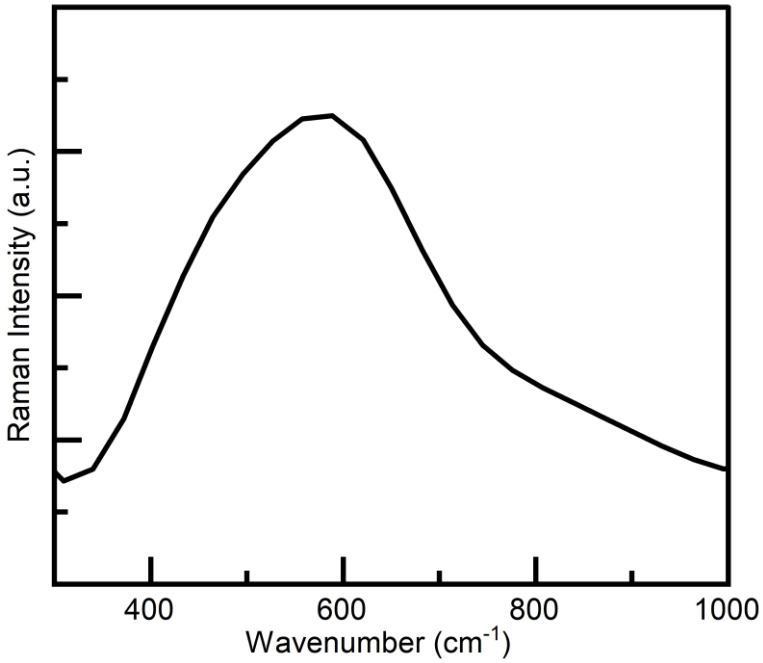

Figure 4.5: Raman spectrum of MoS_2 extracted from a hyperspectral image.

4.1.2 Photoluminescence characteristics of FL-MoS_2

Molybdenum disulfide (MoS_2), a layered two-dimensional (2D) material, has gained significant attention due to its unique electronic and optical properties, particularly its strong PL in the monolayer form. MoS_2 exhibits direct bandgap behavior in its monolayer form, allowing efficient absorption and emission of light.[28,78,79] However, the emission intensity significantly decreases as the number of layers increases. The different photoluminescence properties of the

monolayer and FL-MoS_2 nanosheets are consistent with the fact that monolayer MoS_2 has a direct band gap structure, while FL-MoS_2 has an indirect one. When MoS_2 is excited by photons with energy greater than its bandgap, electron-hole pairs are generated.[80] These excitons then recombine, leading to the emission of light. The energy and intensity of this emitted light provide valuable information about the electronic structure, defects, and excitonic properties of the material.[75]

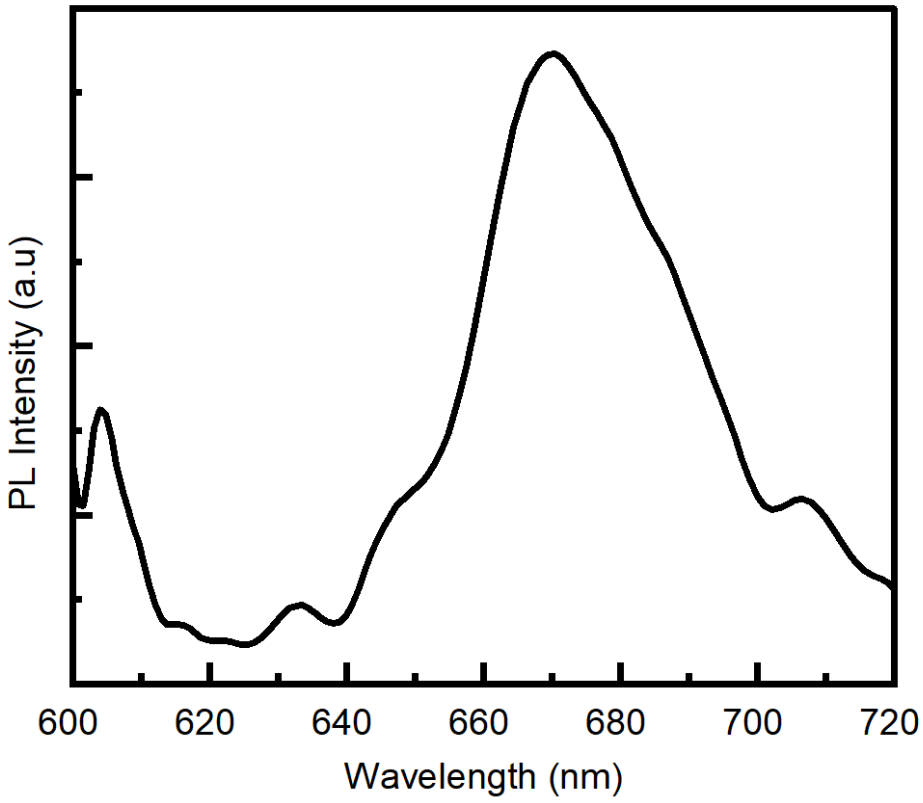

Figure 4.6: PL Spectrum of FL-MoS_2.

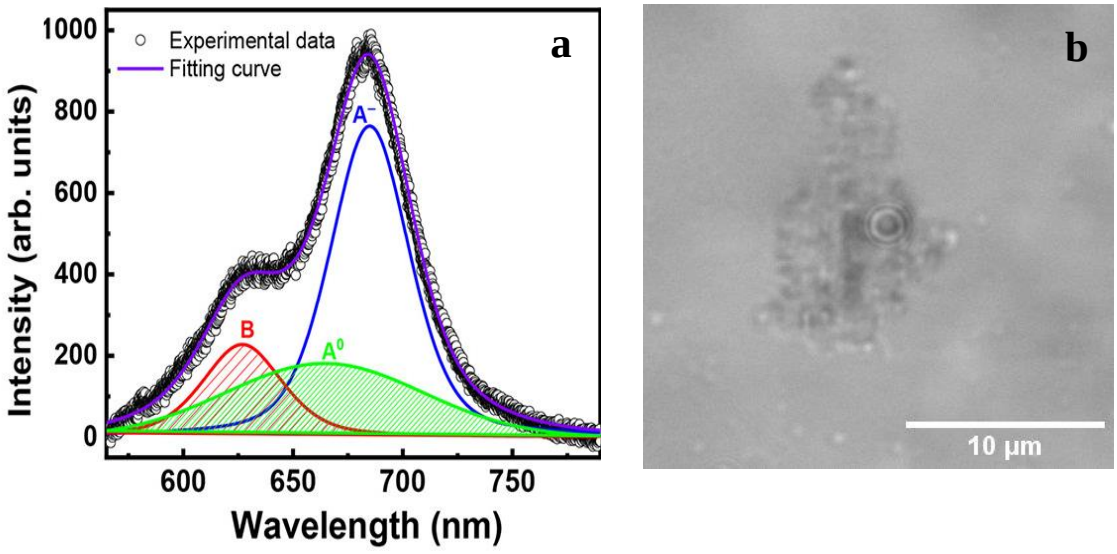

Figure 4.7: a) Typical PL spectrum of mono layer MoS_2 with the exciton peaks and the Trion peak[66] b) Bright field image of electrochemical exfoliated FL-MoS_2.

The photoluminescence spectrum obtained in this study (Figure 4.6) exhibits a broad peak in the visible to near-infrared range, which is dominated by excitonic emissions associated with electronic transitions. The key PL features observed in the spectrum are related to excitons, specifically the A exciton, B exciton, and trions. The A exciton peak corresponds to the direct optical transition between the valence and conduction bands at the K-point in the Brillouin zone.[81] In monolayer MoS_2, this exciton displays strong PL emission around 650–670 nm (Figure 4.7a). In the FL-MoS_2 sample examined, the A exciton remains the dominant feature in the PL spectrum but shows a slight redshift, which can be attributed to increased interlayer coupling. The observed peak for the A exciton was found around 690 nm, indicating the presence of a few layers rather than a monolayer. This redshift is associated with the reduced bandgap as more layers are stacked together. While multilayer MoS_2 is typically dominated by indirect transitions, the FL-MoS_2 sample still exhibits direct excitonic emissions, although they are weaker compared to monolayers. The B exciton, which arises from a spin-orbit split band at the K-point, is another notable feature in the PL spectrum and is typically located at a higher energy (~600 nm in monolayers).[59] In the FL-MoS_2 , the B exciton peak appeared around 635 nm, also showing a small redshift compared to the monolayer spectrum, consistent with the increased layer number. Furthermore, charged excitons or trions can be observed in MoS_2, particularly in doped or defected samples. Trions typically exhibit a small energy shift compared

to neutral excitons. In the FL-MoS_2 sample, a faint shoulder was observed on the lower energy side of the A exciton peak, around ~710 nm, which could be attributed to trions, potentially formed due to residual electron doping from the substrate or environmental factors.[12] Also, the bright field image shows that the lateral size of the exfoliated MoS_2 monolayer flakes is in the 5-15 μm range (Figure 4.7b).

4.2 In-situ electrochemical study of exfoliated MoS_2 nanomaterials

Molybdenum disulfide, a layered transition metal dichalcogenide, is known for its tunable electronic and optical properties. The PL signal of MoS_2, arising from exciton and trion recombination, is highly sensitive to factors such as layer number, defects, and environmental conditions.[58] Therefore, the effect of applied voltage during a reaction process can provide insights into the dynamic nature of the material and the underlying optoelectronic processes. Figure 4.7 shows the total intensity of excitons and trions in NaCl solution. It clearly indicates the heterogeneous flake of MoS_2, with areas of intense PL signals as well as dark areas of weak signals at 0 V. Upon shifting the voltage to -2 V as shown in Figure 4.7a, there are noticeable changes in the photoluminescence intensity. According to the past research when an external potential is applied to MoS_2, the band structure can be dynamically altered through electrostatic doping (either electron or hole doping).[3,16] Therefore, the photoluminescence signal is observed to increase in certain regions of the MoS_2 flake, indicating a voltage-induced modulation of the excitonic and trion recombination processes by the doping. This highlights the dynamic nature of the optoelectronic properties of MoS_2 and the potential for voltage-controlled manipulation of its optical characteristics.

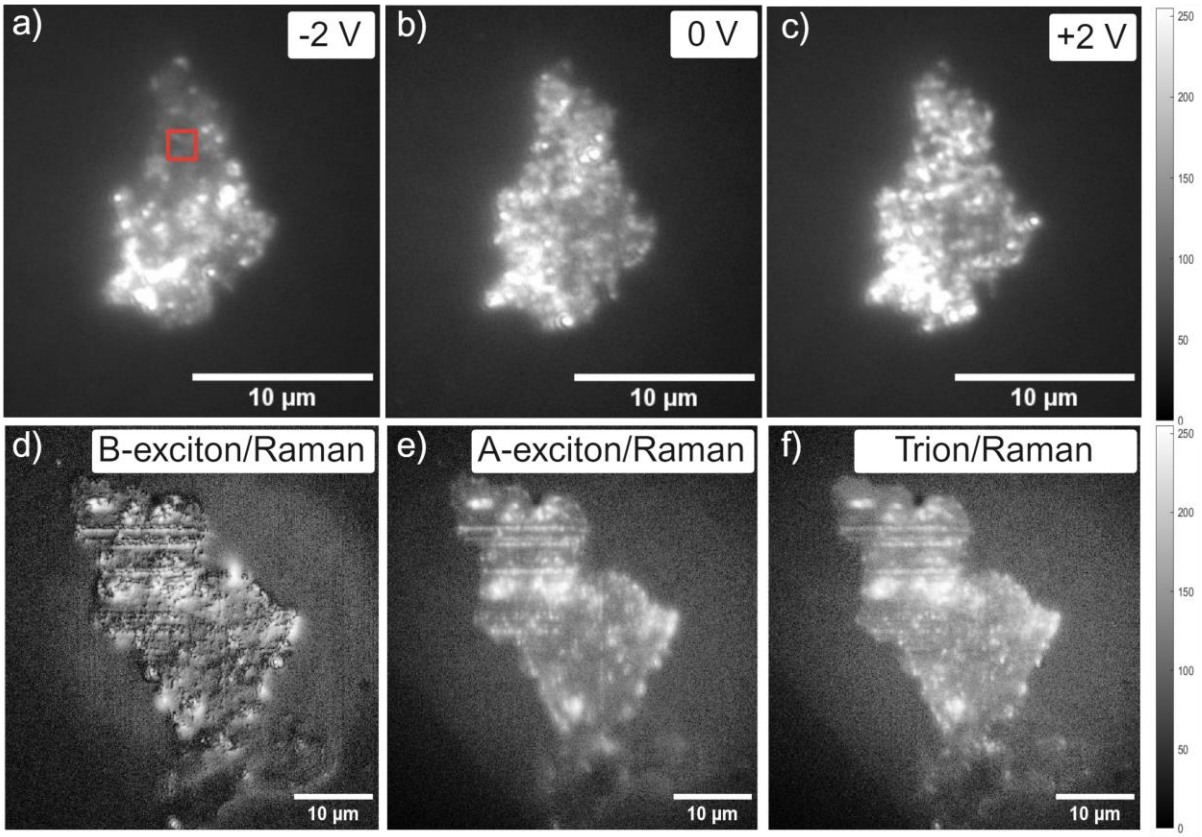

Figure 4.8: Selected FL-MoS_2 flake with applied voltages a) -2 V b) 0 V c) +2 V ; (d-f) Ratio of PL excitons and total Raman signals.

Figures 4.8 (d-f) illustrate the ratio of PL from B-exciton, A-exciton, and trions with the corresponding total Raman signal from the A_{1g} and E^1_{2g} peaks appearing between 400 cm^{-1} and 500 cm^{-1}. As mentioned in the above, Raman signals are stronger from multilayer MoS_2, while PL signals are stronger from FL-MoS_2. Therefore, the ratio can be used to map the FL-MoS_2 regions where a higher ratio signifies 3-4 layers. It is evident from Figures 4.8 (d-f) that an electrochemically exfoliated flake exhibits significant inhomogeneity due to its intrinsic structure. Also, it should be mentioned that due to the poor spectral resolution from the interferometer, total Raman signals intensities from A_{1g} and E^1_{2g} have been considered for the preparation of the above images.

Figure 4.9 and Figure 4.10 represent the false colour representation of the hyperspectral images during the electrochemical reaction using NaCl solution. Those images clearly show considerable PL intensity variation across the MoS_2 flake. It is noted that due to large size of the HSI data, only band intensities are taken into account in this representation (Figure 4.9).

Blue colour corresponds to intensity at 610 nm (B-exciton), green colour corresponding to 650 nm (A-exciton) and red colour corresponding to trions (680 nm). At the applied voltages, the trion intensity can be observed more prominently compared to the 0 V condition. This indicates that the trion PL intensity clearly depends on the applied voltage and can be tuned through electrical control. This finding could be valuable for hydrogen evolution reactions, considering that HER activity depends on the density of available electrons via trions and the binding of the reactants and products onto the trion-rich regions.[77]

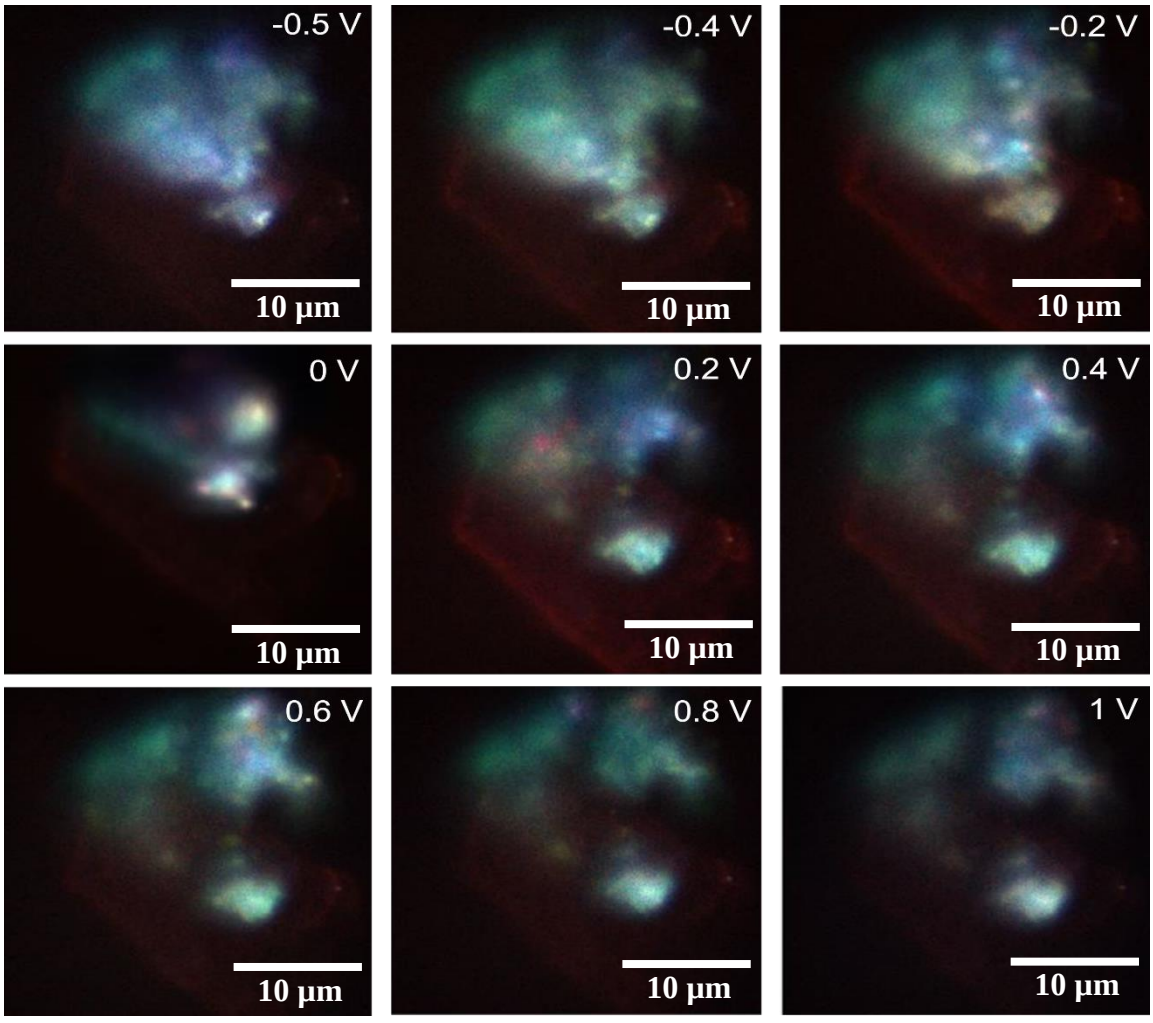

Figure 4.9: False colour HSI images with their respective applied voltages. blue corresponds to B-exciton, green corresponds to A-exciton and red corresponds to trions.

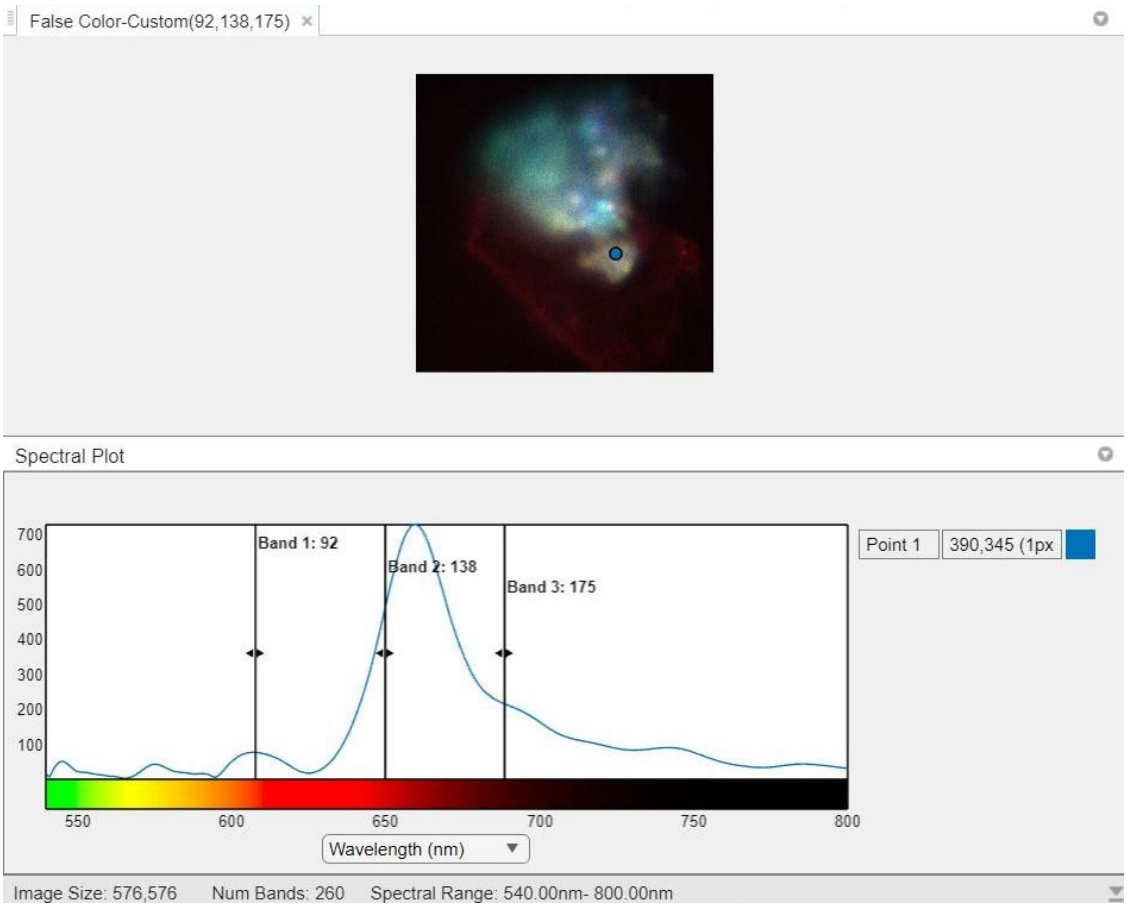

Figure 4.10: Screen captured image while generating the HSI image with the exciton and trion bands. Image shows a PL spectrum of the MoS_2.

To identify the peak positions and their variation with the voltage difference, one area was selected, and the intensity was observed throughout the experiment. Figure 4.11 shows the two plots of three fitted peaks obtained from that selected area. According to the results, most of the A exciton photoluminescence intensity was higher when negative voltages were applied. This observation can be attributed to the fact that applying a negative voltage to MoS_2 introduces additional electrons into the conduction band, resulting in n-type doping.[5,65] This increases the overall electron density in the system, which in turn enhances the A exciton emission. Furthermore, the peak center of the A exciton shifts towards lower energies (Red shift) with increasing negative voltage, suggesting a change in the electronic structure of MoS_2 due to the injection of additional charge carriers.[65] As example, the additional free electrons in the system caused by the negative voltage the A excitons can capture an extra electron and form trions.

This reduces the number of free neutral A excitons, effectively shifting the overall A exciton PL peak. The newly formed trions have lower recombination energy compared to neutral excitons, contributing to a red shift in the spectrum.

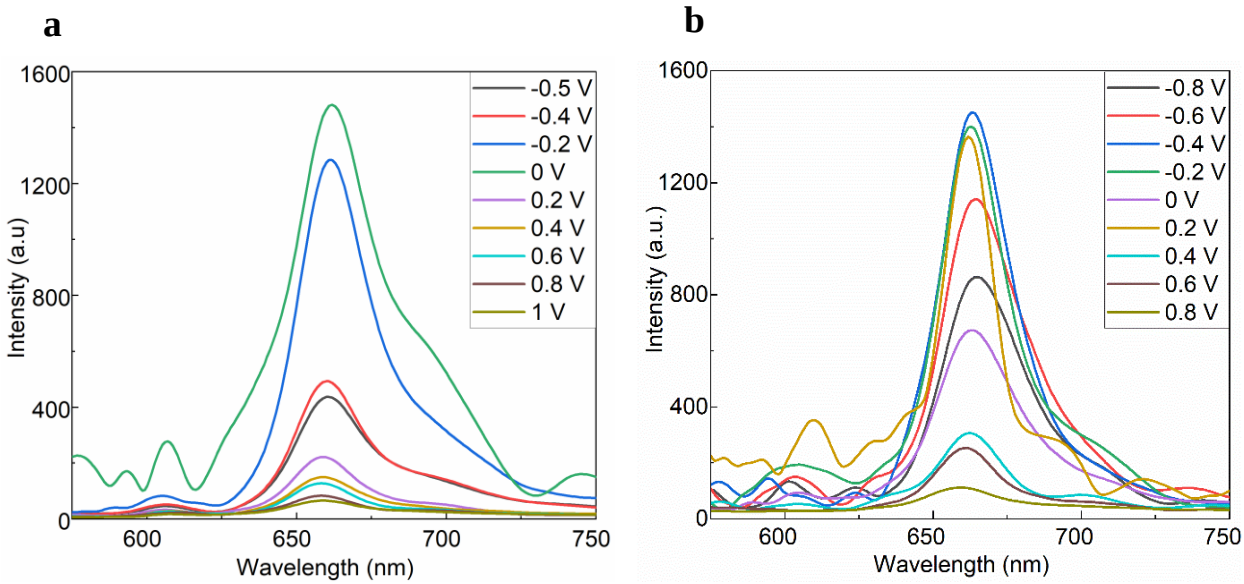

Figure 4.11: Photoluminescence intensity variations with the voltage. The experimentally observed spectrum was fitted using two gaussian functions and a Fano function to deconvolve the spectral peaks. a) NaCl as the electrolyte b) DI water as the electrolyte.

Since the above results suggest that peak width, peak intensity and peak center can give an important information about the overall photoluminescence, the impact of the voltage on exciton dynamics was further investigate. Figure 4.12 shows the plots extracted from a particular region of the hyperspectral images acquired at -0.5 V and +0.6 V. Although the spectra strongly depend on the location and circumstance of the scan, it can be seen from Figure 4.12 that the degree of asymmetry changes during the potential sweep from -0.4 to +0.5 V, which relates to the width of the peak. Change in B-exciton (610 nm) is minimal whereas there is strong variation in the A-exciton. The centre of the trion peak exhibits a blue shift for positive potential and a red shift with negative potential. These observations are consistent with previously reported work using solid-state devices such as field-effect transistors where a back-gate voltage is applied.[9,11,66,82] These two plots are fitted with two symmetric Gaussian functions and one asymmetric function to account for the intensity tail on the low energy side. A Fano resonance function has been previously used to fit such asymmetric PL intensity from trions in

chromium thiophosphate ($CrPS_4$).[83] In this case, the combination of functions fits the spectra at different voltages with high accuracy.

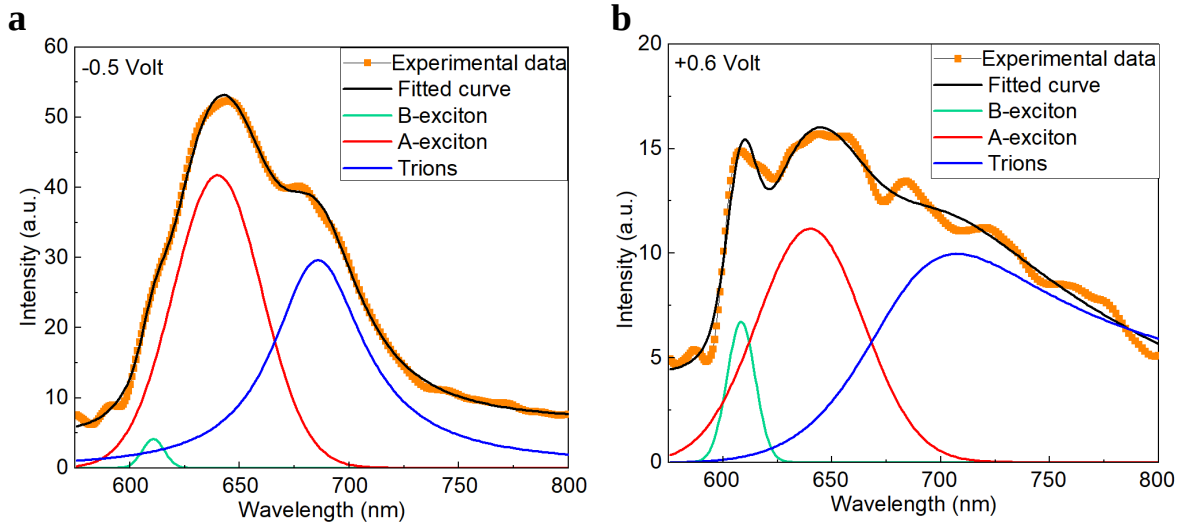

Figure 4.12: The plot of trion intensity extracted from a selected region of the hyperspectral image with a) -0.5 V b) +0.6 V.

Trions are charged excitons formed when an exciton binds with an additional electron or hole. The formation of trions is directly influenced by the electron or hole density in the material.[32,82,84] In MoS_2, applying a voltage during an electrochemical reaction can increase carrier density by adding electrons or holes, leading to a shift from neutral excitons to trions. Therefore, understanding the changes in trion photoluminescence is crucial to explain the voltage dependence on catalysis behaviour of MoS_2. Figure 4.13a and 4.13b shows the plot of trion intensity extracted from a selected region of a images obtained on a different FL-MoS_2 sample (scan rate of 50 mV/s), which were acquired using a bandpass filter (680 ± 5 nm) to isolate the trion intensity.

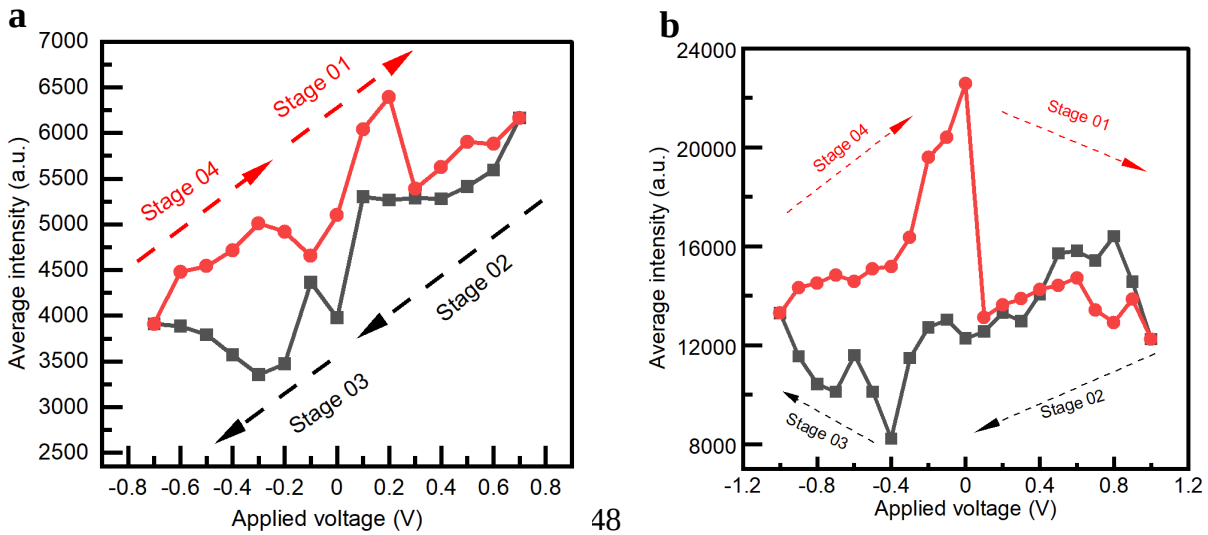

Figure 4.13: The plots of trion intensity in a voltage scan experiment a) NaCl as electrolyte solution b) DI water as the electrolyte solution.

According to the Figure 4.13, it is evident that PL intensity strongly depends on several factors, including the electrical layer formed during the scan. For example, at -0.3 V in NaCl solution, the intensities differ during the upward and downward scans. It is well known that the electrical layer formed during the voltage scan plays a key role in determining the Tafel plot and the overpotential in the hydrogen evolution reaction (HER).[41] Previous such measurements on MoS_2 in an electrochemical cell like ours required fabricating electrodes that connect only to the flake being probed.[42] This process is time-consuming and requires elaborate sample fabrication. Our method provides an alternative to the current-voltage scan by probing the trion-PL intensity variation with voltage. Also, the observed PL intensity is lower when using NaCl as the electrolyte compared to DI water. This could be attributed to the ionic screening effect. In the NaCl electrolyte, the Na^+ and Cl^- ions can screen the charge carriers within the MoS_2 layers.[85] Photoluminescence in MoS_2 arises from the recombination of excitons, and the presence of charged ions in the electrolyte can reduce the Coulomb attraction between the electrons and holes, thereby weakening exciton formation.[19,29,40] This screening effect leads to a reduction in exciton binding energy, ultimately decreasing the overall PL intensity. In contrast, water molecules are much less efficient at screening charges, allowing for stronger excitonic emissions and higher PL intensity.[40]

Throughout the in-situ hyperspectral imaging experiment, stabilising of MoS_2 flake in electrochemical environments, especially with ionic electrolytes, remains a challenge. Because in combination with water, NaCl can sometimes lead to chemical reactions at the MoS_2 surface, especially under electrochemical conditions. Over time, the Na^+ and Cl^- ions may facilitate corrosion or chemical degradation of the MoS_2 surface, particularly at defect sites or edges. This corrosion can create additional surface defects, which act as non-radiative recombination centers, further reducing the PL intensity. Additionally, chloride ions are known to be reactive and could lead to surface etching or chemical modifications of MoS_2 over time, especially under applied potentials or in the presence of dissolved oxygen. This chemical activity could degrade the MoS_2 structure, resulting in reduced PL efficiency during the observations.

CHAPTER 5 - CONCLUSIONS AND FUTURE WORK

FL-MoS_2 nanosheets can be prepared by electrochemically exfoliating the bulk MoS_2 crystal in an ionic solution. The lateral size of the exfoliated MoS_2 flakes can reach up to 30 μm, which is significantly larger compared to those produced by mechanical, chemical, and liquid-phase exfoliation methods. The thickness of the electrochemically exfoliated MoS_2 flakes is typically 3-5 layers, making them suitable for observing the in-situ electrochemical behavior of the material. In the future, it would be beneficial to optimise the electrochemical exfoliation process to produce high-yield mono or bilayer MoS_2 flakes, as these thin structures are expected to exhibit enhanced electronic and optoelectronic properties, which could be leveraged in a wider range of electrochemical applications. Also, traditional characterization method such as XRD, AFM and SEM should implied to get better understanding about the material quality.

Excitons in this case are generated due to both optical excitation by the probing laser and the electrochemical pumping of electrons or holes. Additionally, both positively and negatively charged trions can be present in the same monolayer due to heterogeneity arising from defects, electrical charge-induced doping, mechanical deformation and strain, and compositional heterogeneity. These factors, together with the reacting species, make the electronic states of the excitons and trions highly complex and heterogeneous. Understanding the spatial heterogeneity in FL-MoS_2 can lead to a deeper comprehension of catalytic mechanisms and potential optimisation strategies for enhanced HER performance. Also, Raman spatial resolution of the HSI setup should also improve with further technological advancement such as use of higher birefringence materials in birefringence-based interferometers or highly stabilized Michelson interferometers geometry. The correlation between the PL intensity variations and applied voltages provides insights into the dynamics of excitons and trions under electrochemical conditions, paving the way for future studies to explore the full potential of 2D TMD materials in catalytic applications. Therefore, more extensive research and development of in-situ and operando characterisation techniques with atomic-scale spatial and temporal resolution should be employed to provide more detailed and comprehensive insights into the HER catalytic processes. This will enable the catalytic performance and reaction kinetics on the various active sites to be directly tracked and analysed, which in turn will significantly aid in the development and optimisation of superior electrocatalysts for practical applications.

REFERENCES

(1) Jin, H.; Guo, C.; Liu, X.; Liu, J.; Vasileff, A.; Jiao, Y.; Zheng, Y.; Qiao, S. Z. Emerging Two-Dimensional Nanomaterials for Electrocatalysis. *Chem. Rev.* **2018**, *118* (13), 6337–6408. https://doi.org/10.1021/acs.chemrev.7b00689.

(2) Wang, H.; Yuan, H.; Sae Hong, S.; Li, Y.; Cui, Y. Physical and Chemical Tuning of Two-Dimensional Transition Metal Dichalcogenides. *Chemical Society Reviews*. **2015**, *44* (1), 2664–2680. https://doi.org/10.1039/C4CS00287C.

(3) Fan, F. R.; Wang, R.; Zhang, H.; Wu, W. Emerging Beyond-Graphene Elemental 2D Materials for Energy and Catalysis Applications. *Chemical Society Reviews*. **2021**, *19* (1), 10983–11031. https://doi.org/10.1039/c9cs00821g.

(4) Liu, Y.; Peng, X. Recent Advances of Supercapacitors Based on Two-Dimensional Materials. *Applied Materials Today*. **2017**, *7* (1), 1–12. https://doi.org/10.1016/j.apmt.2017.01.004.

(5) Kirubasankar, B.; Won, Y. S.; Adofo, L. A.; Choi, S. H.; Kim, S. M.; Kim, K. K. Atomic and Structural Modifications of Two-Dimensional Transition Metal Dichalcogenides for Various Advanced Applications. *Chemical Science*, **2022**, *26* (1), 7707–7738. https://doi.org/10.1039/d2sc01398c.

(6) Shanmugam, V.; Mensah, R. A.; Babu, K.; Gawusu, S.; Chanda, A.; Tu, Y.; Neisiany, R. E.; Försth, M.; Sas, G.; Das, O. A Review of the Synthesis, Properties, and Applications of 2D Materials. *Particle and Particle Systems Characterization*. John Wiley and Sons Inc June 1, **2022**. https://doi.org/10.1002/ppsc.202200031.

(7) Grayfer, E. D.; Kozlova, M. N.; Fedorov, V. E. Colloidal 2D Nanosheets of MoS2 and Other Transition Metal Dichalcogenides through Liquid-Phase Exfoliation. *Adv. Colloid Interface Sci.* **2017**, *245* (1), 40–61. https://doi.org/10.1016/J.CIS.2017.04.014.

(8) Wang, H.; Lu, Z.; Kong, D.; Sun, J.; Hymel, T. M.; Cui, Y. Electrochemical Tuning of MoS2 Nanoparticles on Three-Dimensional Substrate for Efficient Hydrogen Evolution. *ACS Nano* **2014**, *8* (5), 4940–4947. https://doi.org/10.1021/nn500959v.

(9) Shepard, G. D.; Ardelean, J. V.; Ajayi, O. A.; Rhodes, D.; Zhu, X.; Hone, J. C.; Strauf, S. Trion-Species-Resolved Quantum Beats in MoSe2. *ACS Nano* **2017**, *11* (11), 11550–11558. https://doi.org/10.1021/acsnano.7b06444.

(10) Philip, A.; Ruban Kumar, A. Recent Advancements and Developments Employing 2D-

Materials in Enhancing the Performance of Electrochemical Supercapacitors: A Review. *Renewable and Sustainable Energy Reviews*. Elsevier Ltd August 1, **2023**, *1* (18), 1-21. https://doi.org/10.1016/j.rser.2023.113423.

(11) Hu, R.; Huang, Z.; Wang, B.; Qiao, H.; Qi, X. Electrochemical Exfoliation of Molybdenum Disulfide Nanosheets for High-Performance Supercapacitors. *J. Mater. Sci. Mater. Electron.* **2021**, *32* (6), 7237–7248. https://doi.org/10.1007/s10854-021-05432-5.

(12) Wang, Y.; Ou, J. Z.; Balendhran, S.; Chrimes, A. F.; Mortazavi, M.; Yao, D. D.; Field, M. R.; Latham, K.; Bansal, V.; Friend, J. R.; Zhuiykov, S.; Medhekar, N. V.; Strano, M. S.; Kalantar-Zadeh, K. Electrochemical Control of Photoluminescence in Two-Dimensional MoS 2 Nanoflakes. *ACS Nano* **2013**, *7* (11), 10083–10093. https://doi.org/10.1021/nn4041987.

(13) Hu, R.; Huang, Z.; Wang, B.; Qiao, H.; Qi, X. Electrochemical Exfoliation of Molybdenum Disulfide Nanosheets for High-Performance Supercapacitors. *J. Mater. Sci. Mater. Electron.* **2021**, *32* (6), 7237–7248. https://doi.org/10.1007/s10854-021-05432-5.

(14) Choi, W.; Choudhary, N.; Han, G. H.; Park, J.; Akinwande, D.; Lee, Y. H. Recent Development of Two-Dimensional Transition Metal Dichalcogenides and Their Applications. *Materials Today*, **2017**, *20* (3), 116–130. https://doi.org/10.1016/j.mattod.2016.10.002.

(15) Dolai, S.; Maiti, P.; Ghorai, A.; Bhunia, R.; Paul, P. K.; Ghosh, D. Exfoliated Molybdenum Disulfide-Wrapped CdS Nanoparticles as a Nano-Heterojunction for Photo-Electrochemical Water Splitting. *ACS Appl. Mater. Interfaces* **2021**, *13* (1), 438–448. https://doi.org/10.1021/acsami.0c16972.

(16) Li, H.; Tsai, C.; Koh, A. L.; Cai, L.; Contryman, A. W.; Fragapane, A. H.; Zhao, J.; Han, H. S.; Manoharan, H. C.; Abild-Pedersen, F.; Nørskov, J. K.; Zheng, X. Activating and Optimizing MoS2 Basal Planes for Hydrogen Evolution through the Formation of Strained Sulphur Vacancies. *Nat. Mater.* **2016**, *15* (1), 48–53. https://doi.org/10.1038/nmat4465.

(17) Ruqia, B.; Kanti Kabiraz, M.; Wook Hong, J.; Choi, S. Il. Catalyst Activation: Surface Doping Effects of Group VI Transition Metal Dichalcogenides towards Hydrogen Evolution Reaction in Acidic Media. *Journal of Energy Chemistry*, **2022**, *72* (1), 217–

240. https://doi.org/10.1016/j.jechem.2022.04.023.

(18) Lv, Y.; Chen, P.; Foo, J. J.; Zhang, J.; Qian, W.; Chen, C.; Ong, W. J. Dimensionality-Dependent MoS2 toward Efficient Photocatalytic Hydrogen Evolution: From Synthesis to Modifications in Doping, Surface and Heterojunction Engineering. *Materials Today Nano*. Elsevier Ltd June 1, **2022**, *18* (1), 1-28. https://doi.org/10.1016/j.mtnano.2022.100191.

(19) Khatua, D. P.; Singh, A.; Gurung, S.; Jayabalan, J. Excitation Density Dependent Carrier Dynamics in a Monolayer MoS2: Exciton Dissociation, Formation and Bottlenecking. *Micro and Nanostructures* **2022**, *165* (1), 1-7. https://doi.org/10.1016/j.micrna.2022.207205.

(20) Kumar, N. A.; Dar, M. A.; Gul, R.; Baek, J. B. Graphene and Molybdenum Disulfide Hybrids: Synthesis and Applications. *Mater. Today* **2015**, *18* (5), 286–298. https://doi.org/10.1016/J.MATTOD.2015.01.016.

(21) Thakur, D.; Porwal, C.; Singh Chauhan, V.; Balakrishnan, V.; Vaish, R. 2D Transition Metal Dichalcogenides: Synthesis Methods and Their Pivotal Role in Photo, Piezo, and Photo-Piezocatalytic Processes. *Sep. Purif. Technol.* **2024**, *337* (1), 1-28. https://doi.org/10.1016/j.seppur.2024.126462.

(22) Liu, N.; Kim, P.; Kim, J. H.; Ye, J. H.; Kim, S.; Lee, C. J. Large-Area Atomically Thin MoS2 Nanosheets Prepared Using Electrochemical Exfoliation. *ACS Nano* **2014**, *8* (7), 6902–6910. https://doi.org/10.1021/nn5016242.

(23) Afanasiev, P. Synthetic Approaches to the Molybdenum Sulfide Materials. *Comptes Rendus Chim.* **2008**, *11* (1–2), 159–182. https://doi.org/10.1016/j.crci.2007.04.009.

(24) Lu, Z.; Lin, Q.; Cao, Z.; Li, W.; Gong, J.; Wang, Y.; Hu, K.; Hu, X. MoS2 Nanomaterials as Lubricant Additives: A Review. *Lubricants*, **2023**, *11* (12), 1-27. https://doi.org/10.3390/lubricants11120527.

(25) Naz, R.; Rasheed, T.; Khan, S.; Bilal, M. Nanostructured 2D Transition Metal Dichalcogenides (TMDs) as Electrodes for Supercapacitor. In *Nanostructured Materials for Supercapacitors*; Thomas, S., Gueye, A. B., Gupta, R. K., Eds.; Springer International Publishing: Cham, **2022**, 319–339. https://doi.org/10.1007/978-3-030-99302-3_15.

(26) Lin, Y. C.; Dumcenco, D. O.; Huang, Y. S.; Suenaga, K. Atomic Mechanism of the Semiconducting-to-Metallic Phase Transition in Single-Layered MoS 2. *Nat. Nanotechnol.* **2014**, *9* (5), 391–396. https://doi.org/10.1038/nnano.2014.64.

(27) Su, L.; Zhang, Y.; Yu, Y.; Cao, L. Dependence of Coupling of Quasi 2-D MoS2 with Substrates on Substrate Types, Probed by Temperature Dependent Raman Scattering. *Nanoscale* **2014**, *6* (9), 4920–4927. https://doi.org/10.1039/c3nr06462j.

(28) Yazdani, S.; Yarali, M.; Cha, J. J. Recent Progress on in-situ Characterizations of Electrochemically Intercalated Transition Metal Dichalcogenides. *Nano Research*, **2019**, *12* (1), 2126–2139. https://doi.org/10.1007/s12274-019-2408-6.

(29) Mak, K. F.; He, K.; Lee, C.; Lee, G. H.; Hone, J.; Heinz, T. F.; Shan, J. Tightly Bound Trions in Monolayer MoS 2. *Nat. Mater.* **2013**, *12* (3), 207–211. https://doi.org/10.1038/nmat3505.

(30) Kiriya, D.; Lobaccaro, P.; Nyein, H. Y. Y.; Taheri, P.; Hettick, M.; Shiraki, H.; Sutter-Fella, C. M.; Zhao, P.; Gao, W.; Maboudian, R.; Ager, J. W.; Javey, A. General Thermal Texturization Process of MoS2 for Efficient Electrocatalytic Hydrogen Evolution Reaction. *Nano Lett.* **2016**, *16* (7), 4047–4053. https://doi.org/10.1021/acs.nanolett.6b00569.

(31) McCreary, K. M.; Hanbicki, A. T.; Sivaram, S. V.; Jonker, B. T. A- and B-Exciton Photoluminescence Intensity Ratio as a Measure of Sample Quality for Transition Metal Dichalcogenide Monolayers. *APL Mater.* **2018**, *6* (11), 1-9. https://doi.org/10.1063/1.5053699.

(32) Xie, J.; Zhang, H.; Li, S.; Wang, R.; Sun, X.; Zhou, M.; Zhou, J.; Lou, X. W.; Xie, Y. Defect-Rich MoS2 Ultrathin Nanosheets with Additional Active Edge Sites for Enhanced Electrocatalytic Hydrogen Evolution. *Adv. Mater.* **2013**, *25* (40), 5807–5813. https://doi.org/10.1002/adma.201302685.

(33) Grayfer, E. D.; Kozlova, M. N.; Fedorov, V. E. Colloidal 2D Nanosheets of MoS2 and Other Transition Metal Dichalcogenides through Liquid-Phase Exfoliation. *Adv. Colloid Interface Sci.* **2017**, *245* (1), 40–61. https://doi.org/10.1016/J.CIS.2017.04.014.

(34) Tsai, C.; Chan, K.; Nørskov, J. K.; Abild-Pedersen, F. Theoretical Insights into the Hydrogen Evolution Activity of Layered Transition Metal Dichalcogenides. *Surf. Sci.* **2015**, *640* (1), 133–140. https://doi.org/10.1016/j.susc.2015.01.019.

(35) Zhang, Q.; Wang, W.; Zhang, J.; Zhu, X.; Zhang, Q.; Zhang, Y.; Ren, Z.; Song, S.; Wang, J.; Ying, Z.; Wang, R.; Qiu, X.; Peng, T.; Fu, L. Highly Efficient Photocatalytic Hydrogen Evolution by ReS2 via a Two-Electron Catalytic Reaction. *Adv. Mater.* **2018**, *30* (23), 1-7. https://doi.org/10.1002/adma.201707123.

(36) Balan, B.; Xavier, M. M.; Mathew, S. MoS2-Based Nanocomposites for Photocatalytic Hydrogen Evolution and Carbon Dioxide Reduction. *ACS Omega*, **2023**, *8* (29), 25649–25673. https://doi.org/10.1021/acsomega.3c02084.

(37) Noh, S. H.; Hwang, J.; Kang, J.; Seo, M. H.; Choi, D.; Han, B. Tuning the Catalytic Activity of Heterogeneous Two-Dimensional Transition Metal Dichalcogenides for Hydrogen Evolution. *J. Mater. Chem. A* **2018**, *6* (41), 20005–20014. https://doi.org/10.1039/c8ta07141a.

(38) Pak, S.; Lim, J.; Hong, J.; Cha, S. Enhanced Hydrogen Evolution Reaction in Surface Functionalized Mos2 Monolayers. *Catalysts* **2021**, *11* (1), 1–9. https://doi.org/10.3390/catal11010070.

(39) Xia, Y.; Huang, J.; Wu, W.; Zhang, Y.; Wang, H.; Zhu, J.; Yao, J.; Xu, L.; Sun, Y.; Zhang, L.; Lu, R.; Xiong, J.; Zou, G. Sulfur-Doped Rhenium Selenide Vertical Nanosheets: A High-Performance Electrocatalyst for Hydrogen Evolution. *ChemCatChem* **2018**, *10* (19), 4424–4430. https://doi.org/10.1002/cctc.201800757.

(40) Kumar, R.; Mishra, V.; Dixit, T.; Barman, P. K.; Nayak, P. K.; Rao, M. S. R. Observation of Positive Trions in α-MoO3/MoS2 van Der Waals Heterostructures. *Nanoscale* **2023**, *15* (29), 12358–12365. https://doi.org/10.1039/d3nr01480k.

(41) Li, L.; Zhang, D.; Gao, Y.; Deng, J.; Gou, Y.; Fang, J. Electric Field Driven Exfoliation of MoS2. *Journal of Alloys and Compounds*, **2021**, *862* (1), 1-11. https://doi.org/10.1016/j.jallcom.2020.158551.

(42) Hsiao, F. H.; Chung, C. C.; Chiang, C. H.; Feng, W. N.; Tzeng, W. Y.; Lin, H. M.; Tu, C. M.; Wu, H. L.; Wang, Y. H.; Woon, W. Y.; Chen, H. C.; Chen, C. H.; Lo, C. Y.; Lai, M. H.; Chang, Y. M.; Lu, L. S.; Chang, W. H.; Chen, C. W.; Luo, C. W. Using Exciton/Trion Dynamics to Spatially Monitor the Catalytic Activities of MoS2 during the Hydrogen Evolution Reaction. *ACS Nano* **2022**, *16* (3), 4298–4307. https://doi.org/10.1021/acsnano.1c10380.

(43) Liu, X.; Li, B.; Li, X.; Harutyunyan, A. R.; Hone, J.; Esposito, D. V. The Critical Role of Electrolyte Gating on the Hydrogen Evolution Performance of Monolayer MoS2. *Nano Lett.* **2019**, *19* (11), 8118–8124. https://doi.org/10.1021/acs.nanolett.9b03337.

(44) Xie, J.; Zhang, J.; Li, S.; Grote, F.; Zhang, X.; Zhang, H.; Wang, R.; Lei, Y.; Pan, B.; Xie, Y. Controllable Disorder Engineering in Oxygen-Incorporated MoS2 Ultrathin Nanosheets for Efficient Hydrogen Evolution. *J. Am. Chem. Soc.* **2013**, *135* (47), 17881–

17888. https://doi.org/10.1021/ja408329q.

(45) Shi, Y.; Zhou, W.; Lu, A. Y.; Fang, W.; Lee, Y. H.; Hsu, A. L.; Kim, S. M.; Kim, K. K.; Yang, H. Y.; Li, L. J.; Idrobo, J. C.; Kong, J. Van Der Waals Epitaxy of MoS 2 Layers Using Graphene as Growth Templates. *Nano Lett.* **2012**, *12* (6), 2784–2791. https://doi.org/10.1021/nl204562j.

(46) Fei, H.; Liu, R.; Zhang, Y.; Wang, H.; Wang, M.; Wang, S.; Ni, M.; Wu, Z.; Wang, J. Extending MoS2-Based Materials into the Catalysis of Non-Acidic Hydrogen Evolution: Challenges, Progress, and Perspectives. *Materials Futures*, **2023**, *2* (1), 1-25. https://doi.org/10.1088/2752-5724/acc51d.

(47) Ganguly, P.; Harb, M.; Cao, Z.; Cavallo, L.; Breen, A.; Dervin, S.; Dionysiou, D. D.; Pillai, S. C. 2D Nanomaterials for Photocatalytic Hydrogen Production. *ACS Energy Lett.* **2019**, *4* (7), 1687–1709. https://doi.org/10.1021/acsenergylett.9b00940.

(48) Gao, G.; Jiao, Y.; Ma, F.; Jiao, Y.; Waclawik, E.; Du, A. Charge Mediated Semiconducting-to-Metallic Phase Transition in Molybdenum Disulfide Monolayer and Hydrogen Evolution Reaction in New 1T′ Phase. *J. Phys. Chem. C* **2015**, *119* (23), 13124–13128. https://doi.org/10.1021/acs.jpcc.5b04658.

(49) Dolai, S.; Maiti, P.; Ghorai, A.; Bhunia, R.; Paul, P. K.; Ghosh, D. Exfoliated Molybdenum Disulfide-Wrapped CdS Nanoparticles as a Nano-Heterojunction for Photo-Electrochemical Water Splitting. *ACS Appl. Mater. Interfaces* **2021**, *13* (1), 438–448. https://doi.org/10.1021/acsami.0c16972.

(50) Meng, C.; Chen, X.; Gao, Y.; Zhao, Q.; Kong, D.; Lin, M.; Chen, X.; Li, Y.; Zhou, Y. Recent Modification Strategies of MoS2 for Enhanced Electrocatalytic Hydrogen Evolution. *Molecules* **2020**, *25* (5), 1–18. https://doi.org/10.3390/molecules25051136.

(51) Toh, R. J.; Sofer, Z.; Luxa, J.; Sedmidubský, D.; Pumera, M. 3R Phase of MoS2 and WS2 Outperforms the Corresponding 2H Phase for Hydrogen Evolution. *Chem. Commun.* **2017**, *53* (21), 3054–3057. https://doi.org/10.1039/C6CC09952A.

(52) Santra, S.; Ali, M. S.; Karmakar, S.; Chattopadhyay, D. Molybdenum Disulfide: A Nanomaterial That Is Paving the Way toward a Sustainable Future. *Mater. Today Sustain.* **2024**, *25 (1),* 1-21. https://doi.org/https://doi.org/10.1016/j.mtsust.2023.100659.

(53) Thomas, N.; Mathew, S.; Nair, K. M.; O'Dowd, K.; Forouzandeh, P.; Goswami, A.; McGranaghan, G.; Pillai, S. C. 2D MoS2: Structure, Mechanisms, and Photocatalytic Applications. *Mater. Today Sustain.* **2021**, *13 (1),* 1-16.

https://doi.org/10.1016/j.mtsust.2021.100073.

(54) Lee, Y.-H.; Zhang, X.-Q.; Zhang, W.; Chang, M.-T.; Lin, C.-T.; Chang, K.-D.; Yu, Y.-C.; Wang, J. T.-W.; Chang, C.-S.; Li, L.-J.; Lin, T.-W. Synthesis of Large-Area MoS2 Atomic Layers with Chemical Vapor Deposition. *Adv. Mater.* **2012**, *24* (17), 2320–2325. https://doi.org/https://doi.org/10.1002/adma.201104798.

(55) Zhao, W.; Pan, J.; Fang, Y.; Che, X.; Wang, D.; Bu, K.; Huang, F. Metastable MoS2: Crystal Structure, Electronic Band Structure, Synthetic Approach and Intriguing Physical Properties. *Chem. – A Eur. J.* **2018**, *24* (60), 15942–15954. https://doi.org/https://doi.org/10.1002/chem.201801018.

(56) Regasa, M. B.; Nyokong, T. Advantages of Electrochemical Exfoliation Method Over Conventional Methods. In *Electrochemical Exfoliation of Graphene and Its Derivatives: Commercial Applications*; Khan, R., Kumar, N., Sadique, M. A., Parihar, A., Eds.; Springer Nature Singapore: Singapore, **2024**, 33–59. https://doi.org/10.1007/978-981-97-2128-3_2.

(57) Leisgang, N.; Shree, S.; Paradisanos, I.; Sponfeldner, L.; Robert, C.; Lagarde, D.; Balocchi, A.; Watanabe, K.; Taniguchi, T.; Marie, X.; Warburton, R. J.; Gerber, I. C.; Urbaszek, B. Giant Stark Splitting of an Exciton in Bilayer MoS2. *Nat. Nanotechnol.* **2020**, *15* (11), 901–907. https://doi.org/10.1038/s41565-020-0750-1.

(58) He, Z.; Zhao, R.; Chen, X.; Chen, H.; Zhu, Y.; Su, H.; Huang, S.; Xue, J.; Dai, J.; Cheng, S.; Liu, M.; Wang, X.; Chen, Y. Defect Engineering in Single-Layer MoS 2 Using Heavy Ion Irradiation. *ACS Appl. Mater. Interfaces* **2018**, *10* (49), 42524–42533. https://doi.org/10.1021/acsami.8b17145.

(59) Voiry, D.; Salehi, M.; Silva, R.; Fujita, T.; Chen, M.; Asefa, T.; Shenoy, V. B.; Eda, G.; Chhowalla, M. Conducting MoS2 Nanosheets as Catalysts for Hydrogen Evolution Reaction. *Nano Lett.* **2013**, *13* (12), 6222–6227. https://doi.org/10.1021/nl403661s.

(60) Pradeepa, H. L.; Mondal, P.; Bid, A.; Basu, J. K. Electrical and Chemical Tuning of Exciton Lifetime in Monolayer MoS2 for Field-Effect Transistors. *ACS Appl. Nano Mater.* **2020**, *3* (1), 641–647. https://doi.org/10.1021/acsanm.9b02170.

(61) Golovynskyi, S.; Irfan, I.; Bosi, M.; Seravalli, L.; Datsenko, O. I.; Golovynska, I.; Li, B.; Lin, D.; Qu, J. Exciton and Trion in Few-Layer MoS2: Thickness- and Temperature-Dependent Photoluminescence. *Appl. Surf. Sci.* **2020**, *515 (1)*, 1-7. https://doi.org/10.1016/j.apsusc.2020.146033.

(62) Cao, Y. Roadmap and Direction toward High-Performance MoS2Hydrogen Evolution Catalysts. *ACS Nano*, **2021**, *15* (7), 11014–11039. https://doi.org/10.1021/acsnano.1c01879.

(63) Drüppel, M.; Deilmann, T.; Krüger, P.; Rohlfing, M. Diversity of Trion States and Substrate Effects in the Optical Properties of an MoS2 Monolayer. *Nat. Commun.* **2017**, *8* (1), 1-7. https://doi.org/10.1038/s41467-017-02286-6.

(64) Liu, X.; Li, B.; Li, X.; Harutyunyan, A. R.; Hone, J.; Esposito, D. V. The Critical Role of Electrolyte Gating on the Hydrogen Evolution Performance of Monolayer MoS2. *Nano Lett.* **2019**, *19* (11), 8118–8124. https://doi.org/10.1021/acs.nanolett.9b03337.

(65) Mouri, S.; Miyauchi, Y.; Matsuda, K. Tunable Photoluminescence of Monolayer MoS2 via Chemical Doping. *Nano Lett.* **2013**, *13* (12), 5944–5948. https://doi.org/10.1021/nl403036h.

(66) Ross, J. S.; Wu, S.; Yu, H.; Ghimire, N. J.; Jones, A. M.; Aivazian, G.; Yan, J.; Mandrus, D. G.; Xiao, D.; Yao, W.; Xu, X. Electrical Control of Neutral and Charged Excitons in a Monolayer Semiconductor. *Nat. Commun.* **2013**, *4 (1)*, 1-6. https://doi.org/10.1038/ncomms2498.

(67) Mak, K. F.; He, K.; Shan, J.; Heinz, T. F. Control of Valley Polarization in Monolayer MoS2 by Optical Helicity. *Nat. Nanotechnol.* **2012**, *7* (8), 494–498. https://doi.org/10.1038/nnano.2012.96.

(68) Bruix, A.; Füchtbauer, H. G.; Tuxen, A. K.; Walton, A. S.; Andersen, M.; Porsgaard, S.; Besenbacher, F.; Hammer, B.; Lauritsen, J. V. In-situ Detection of Active Edge Sites in Single-Layer MoS2 Catalysts. *ACS Nano* **2015**, *9* (9), 9322–9330. https://doi.org/10.1021/acsnano.5b03199.

(69) Topsøe, H. Developments in Operando Studies and in-situ Characterization of Heterogeneous Catalysts. In *Journal of Catalysis*, **2003**, *216* (2), 155–164. https://doi.org/10.1016/S0021-9517(02)00133-1.

(70) Chen, W.; Wang, J.; Wan, F.; Wang, P. Review of Optical Fibre Sensors for Electrical Equipment Characteristic State Parameters Detection. *High Volt.* **2019**, *4* (4), 271–281. https://doi.org/https://doi.org/10.1049/hve.2019.0157.

(71) Cialla-May, D.; Schmitt, M.; Popp, J. Miniaturized Raman Instruments for SERS-Based Point-of-Care Testing on Respiratory Viruses, *Phys. Sci. Rev.* **2019**, *4* (6), 1-31. https://doi.org/doi:10.1515/psr-2017-0040.

(72) Prochazka, M. Basics of Raman Scattering (RS) Spectroscopy. In *Surface-Enhanced Raman Spectroscopy: Bioanalytical, Biomolecular and Medical Applications*; Springer International Publishing: Cham, **2016**, 7–19. https://doi.org/10.1007/978-3-319-23992-7_2.

(73) Alhalaby, H.; Zaraket, H.; Principe, M. Enhanced Photoluminescence with Dielectric Nanostructures: A Review. *Results Opt.* **2021**, *3 (1),* 1-13. https://doi.org/https://doi.org/10.1016/j.rio.2021.100073.

(74) Li, Q.; Anpo, M.; You, J.; Yan, T.; Wang, X. Photoluminescence (PL) Spectroscopy. In *Springer Handbook of Advanced Catalyst Characterization*; Wachs, I. E., Bañares, M. A., Eds.; Springer International Publishing: Cham, **2023**, 295–321. https://doi.org/10.1007/978-3-031-07125-6_14.

(75) Ye, M.; Winslow, D.; Zhang, D.; Pandey, R.; Yap, Y. K. Recent Advancement on the Optical Properties of Two-Dimensional Molybdenum Disulfide (MoS2) Thin Films. *Photonics* **2015**, *2* (1), 288–307. https://doi.org/10.3390/photonics2010288.

(76) Khan, M. J.; Khan, H. S.; Yousaf, A.; Khurshid, K.; Abbas, A. Modern Trends in Hyperspectral Image Analysis: A Review. *IEEE Access*, **2018**, *6* (1), 14118–14129. https://doi.org/10.1109/ACCESS.2018.2812999.

(77) Huang, T. X.; Cong, X.; Wu, S. S.; Wu, J. Bin; Bao, Y. F.; Cao, M. F.; Wu, L.; Lin, M. L.; Wang, X.; Tan, P. H.; Ren, B. Visualizing the Structural Evolution of Individual Active Sites in MoS2 during Electrocatalytic Hydrogen Evolution Reaction. *Nat. Catal.* **2024**, *7* (6), 646–654. https://doi.org/10.1038/s41929-024-01148-x.

(78) Singh, A.; Moody, G.; Tran, K.; Scott, M. E.; Overbeck, V.; Berghäuser, G.; Schaibley, J.; Seifert, E. J.; Pleskot, D.; Gabor, N. M.; Yan, J.; Mandrus, D. G.; Richter, M.; Malic, E.; Xu, X.; Li, X. Trion Formation Dynamics in Monolayer Transition Metal Dichalcogenides. *Phys. Rev. B* **2016**, *93* (4), 1–5. https://doi.org/10.1103/PhysRevB.93.041401.

(79) He, Y.; He, Q.; Wang, L.; Zhu, C.; Golani, P.; Handoko, A. D.; Yu, X.; Gao, C.; Ding, M.; Wang, X.; Liu, F.; Zeng, Q.; Yu, P.; Guo, S.; Yakobson, B. I.; Wang, L.; Seh, Z. W.; Zhang, Z.; Wu, M.; Wang, Q. J.; Zhang, H.; Liu, Z. Self-Gating in Semiconductor Electrocatalysis. *Nat. Mater.* **2019**, *18* (10), 1098–1104. https://doi.org/10.1038/s41563-019-0426-0.

(80) Huang, T.-X.; Cong, X.; Wu, S.-S.; Wu, J.-B.; Bao, Y.-F.; Cao, M.-F.; Wu, L.; Lin, M.-

L.; Wang, X.; Tan, P.-H.; Ren, B. Visualizing the Structural Evolution of Individual Active Sites in MoS2 during Electrocatalytic Hydrogen Evolution Reaction. *Nat. Catal.* **2024**, *7* (6), 646–654. https://doi.org/10.1038/s41929-024-01148-x.

(81) Cavalcante, L. S. R.; Da Costa, D. R.; Farias, G. A.; Reichman, D. R.; Chaves, A. Stark Shift of Excitons and Trions in Two-Dimensional Materials. *Phys. Rev. B* **2018**, *98* (24), 1-6. https://doi.org/10.1103/PhysRevB.98.245309.

(82) Wang, Y.; Frisbie, C. D. Four-Terminal Electrochemistry: A Back-Gate Controls the Electrochemica

l Potential of a 2D Working Electrode. *J. Phys. Chem. C* **2023**, *8* (4), 1819-1826. https://doi.org/10.1021/acs.jpcc.3c07198.

(83) Gu, P.; Tan, Q.; Wan, Y.; Li, Z.; Peng, Y.; Lai, J.; Ma, J.; Yao, X.; Yang, S.; Yuan, K.; Sun, D.; Peng, B.; Zhang, J.; Ye, Y. Photoluminescent Quantum Interference in a van Der Waals Magnet Preserved by Symmetry Breaking. *ACS Nano* **2020**, *14* (1), 1003–1010. https://doi.org/10.1021/acsnano.9b08336.

(84) Wang, H.; Zhang, C.; Rana, F. Ultrafast Dynamics of Defect-Assisted Electron-Hole Recombination in Monolayer MoS2. *Nano Lett.* **2015**, *15* (1), 339–345. https://doi.org/10.1021/nl503636c.

(85) Xu, J.; Shao, G.; Tang, X.; Lv, F.; Xiang, H.; Jing, C.; Liu, S.; Dai, S.; Li, Y.; Luo, J.; Zhou, Z. Frenkel-Defected Monolayer MoS2 Catalysts for Efficient Hydrogen Evolution. *Nat. Commun.* **2022**, *13* (1), 1-8. https://doi.org/10.1038/s41467-022-29929-7.

APPENDIX

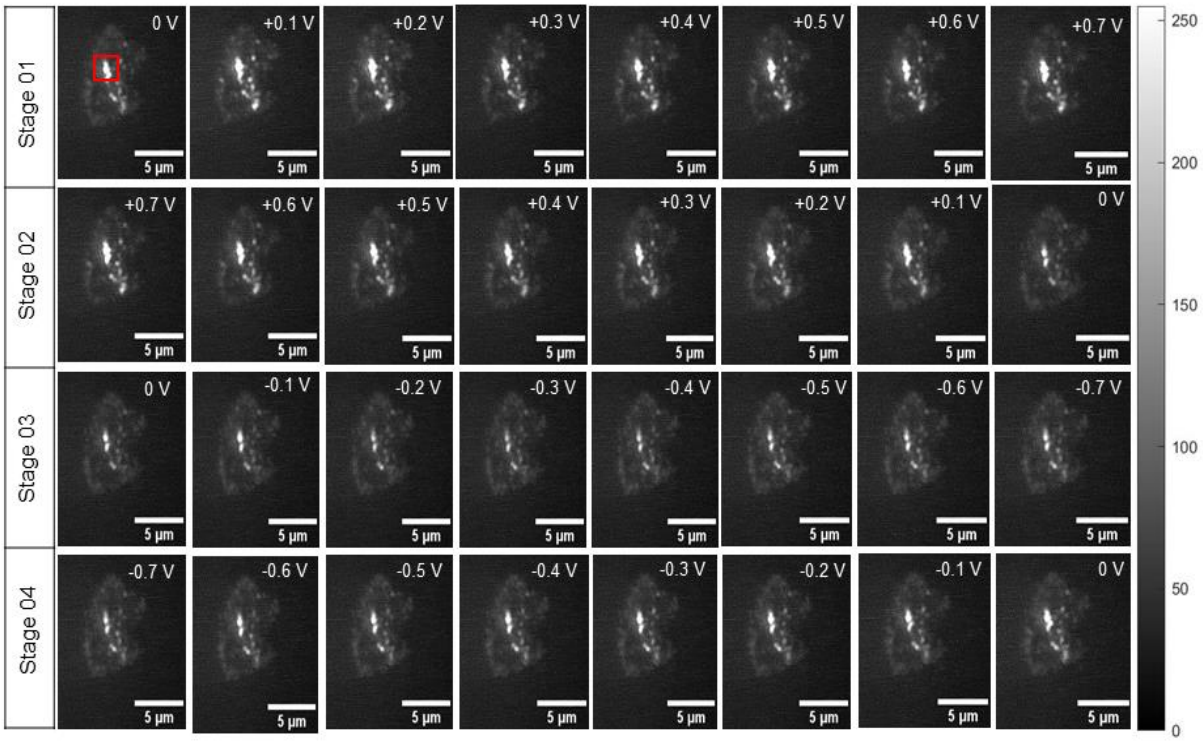

Figure A.0.1: Trion-PL images corresponding to the Figure 4.12a.

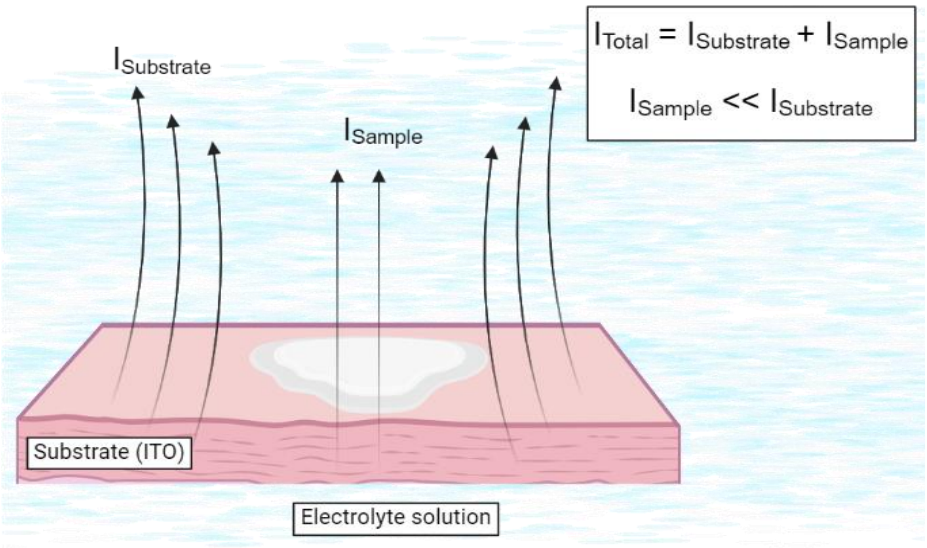

Figure A.0.2: Current flow of the in-situ electrochemical experiment.

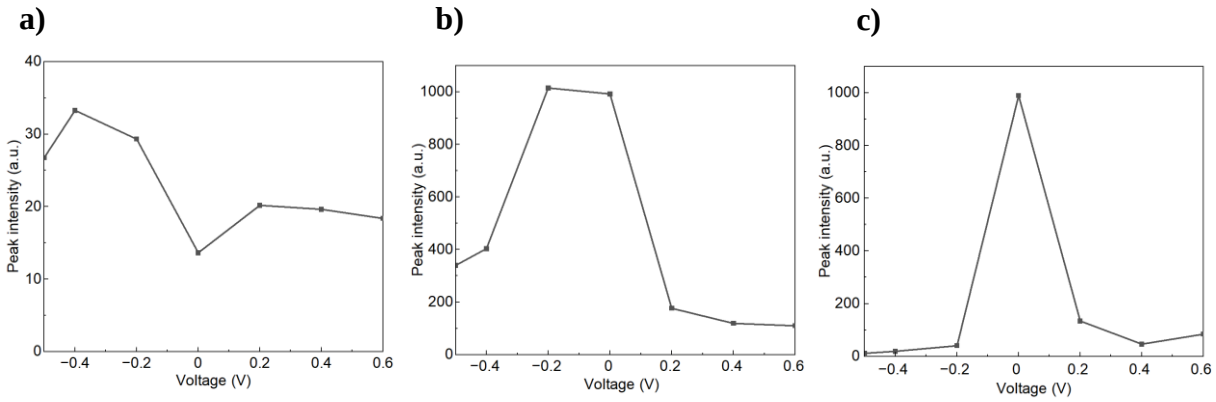

Figure A.0.3: PL peak intensity variation with the voltage. NaCl was used as the electrolyte a) B-exciton b) A-exciton c) Trion.

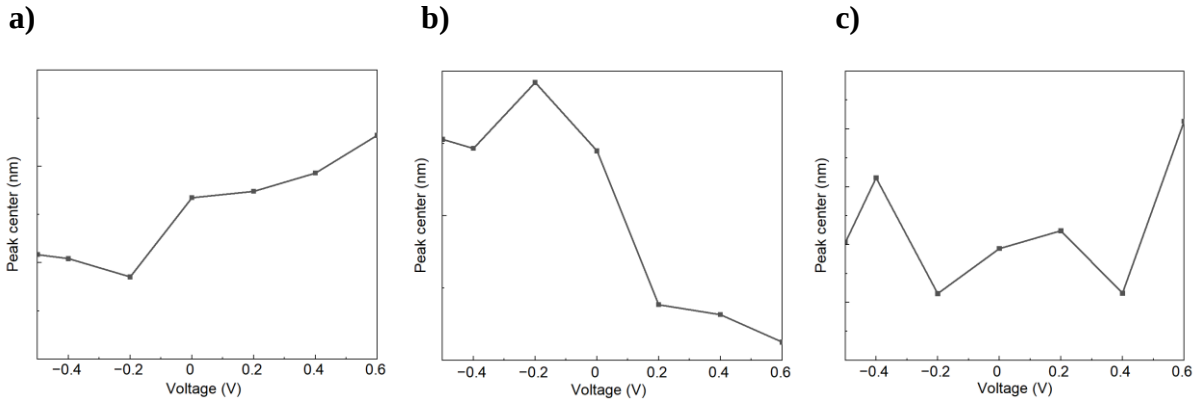

Figure A.0.4: PL peak center variation with the voltage. NaCl was used as the electrolyte a) B-exciton b) A-exciton c) Trion.

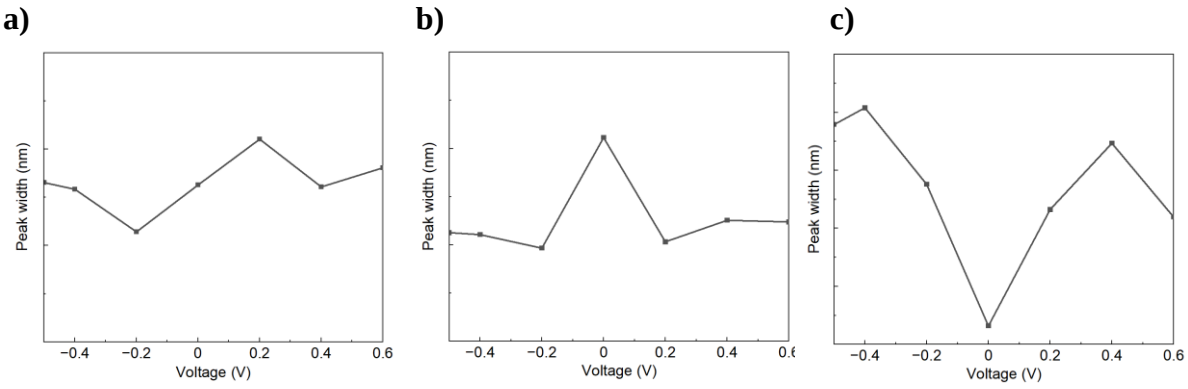

Figure A.0.5: PL peak width variation with the voltage. NaCl was used as the electrolyte a) B-exciton b) A-exciton c) Trion.

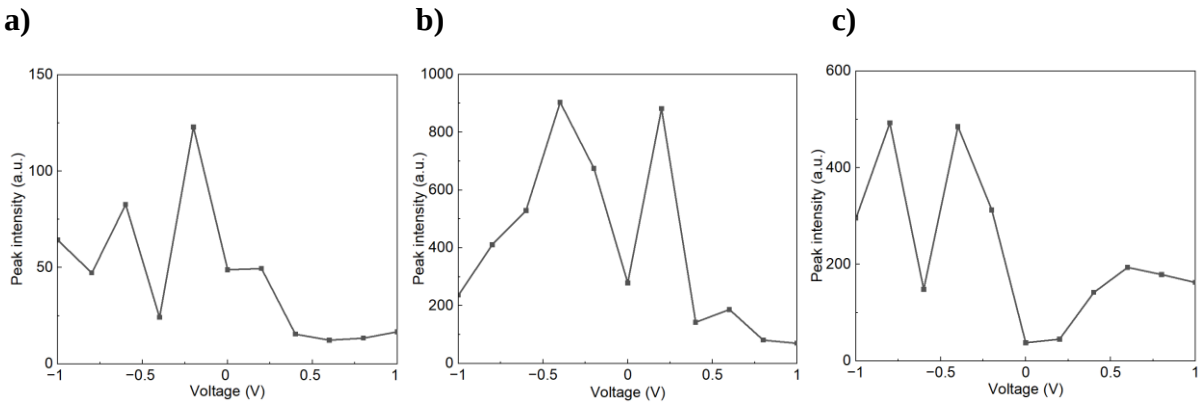

Figure A.0.6: PL peak Intensity variation with the voltage. DI water was used as the electrolyte a) B-exciton b) A-exciton c) Trion.

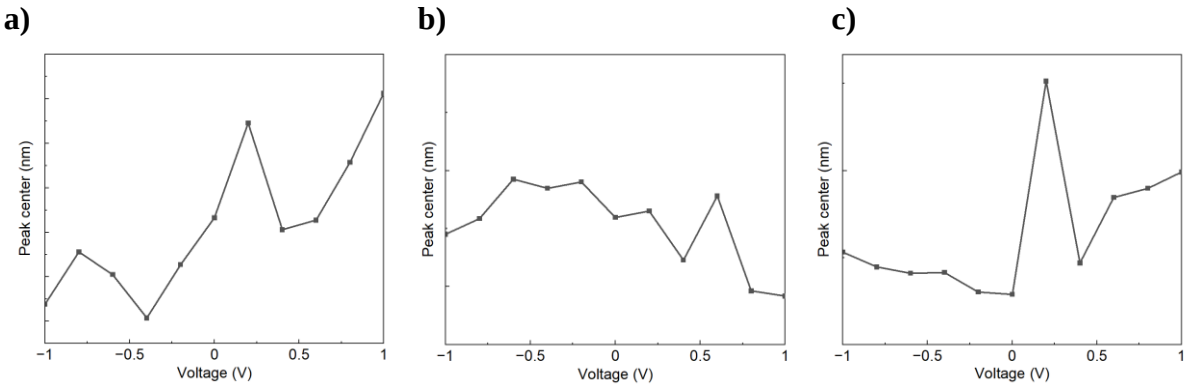

Figure A.0.7: PL peak center variation with the voltage. DI water was used as the electrolyte a) B-exciton b) A-exciton c) Trion.

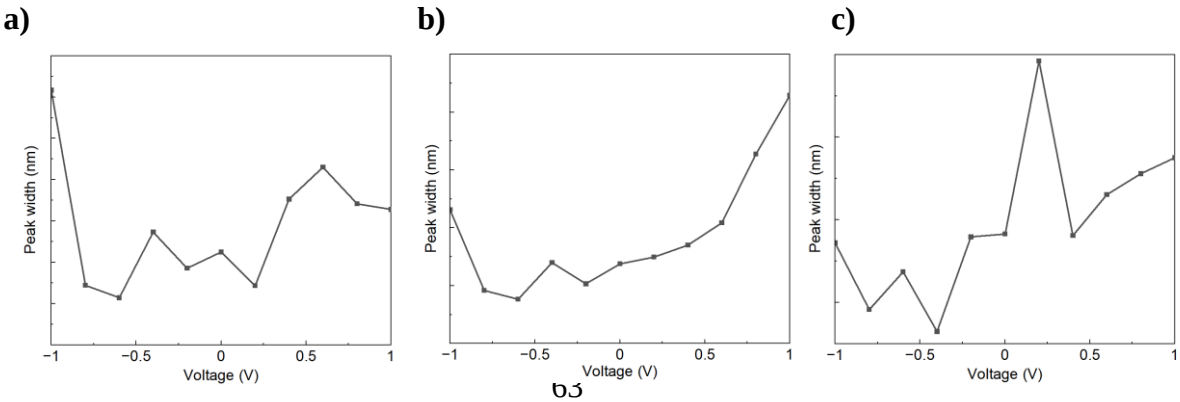

Figure A.0.8: PL peak width variation with the voltage. DI water was used as the electrolyte a) B-exciton b) A-exciton c) Trion.

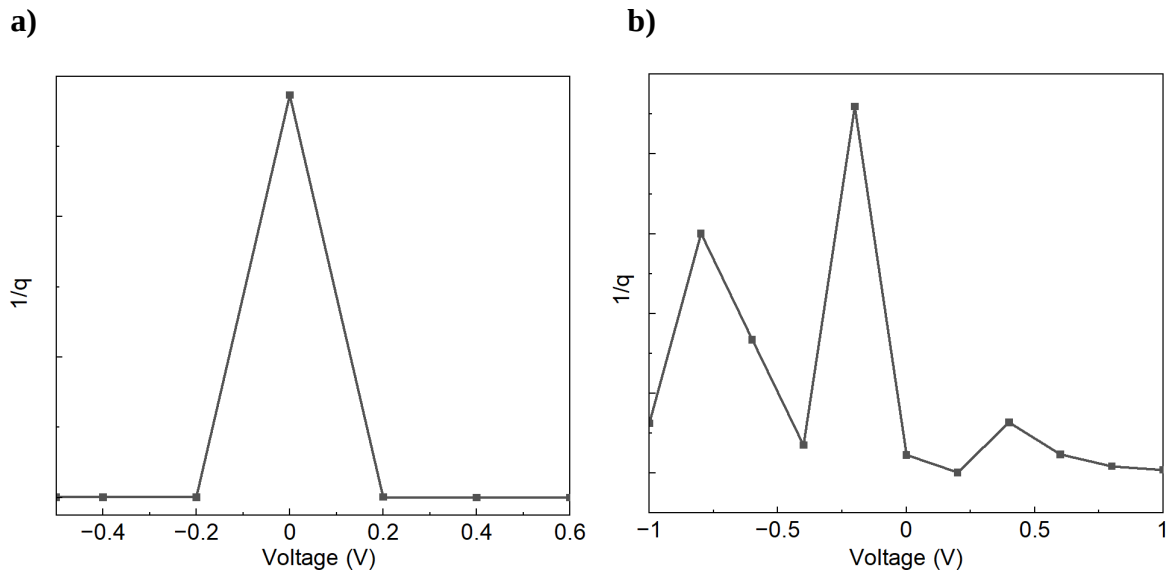

Figure A.0.9: Asymmetric effect of Fano function with voltage a) NaCl as the electrolyte b) DI water as the electrolyte.